CHALMERS
UNIVERSITY OF TECHNOLOGY

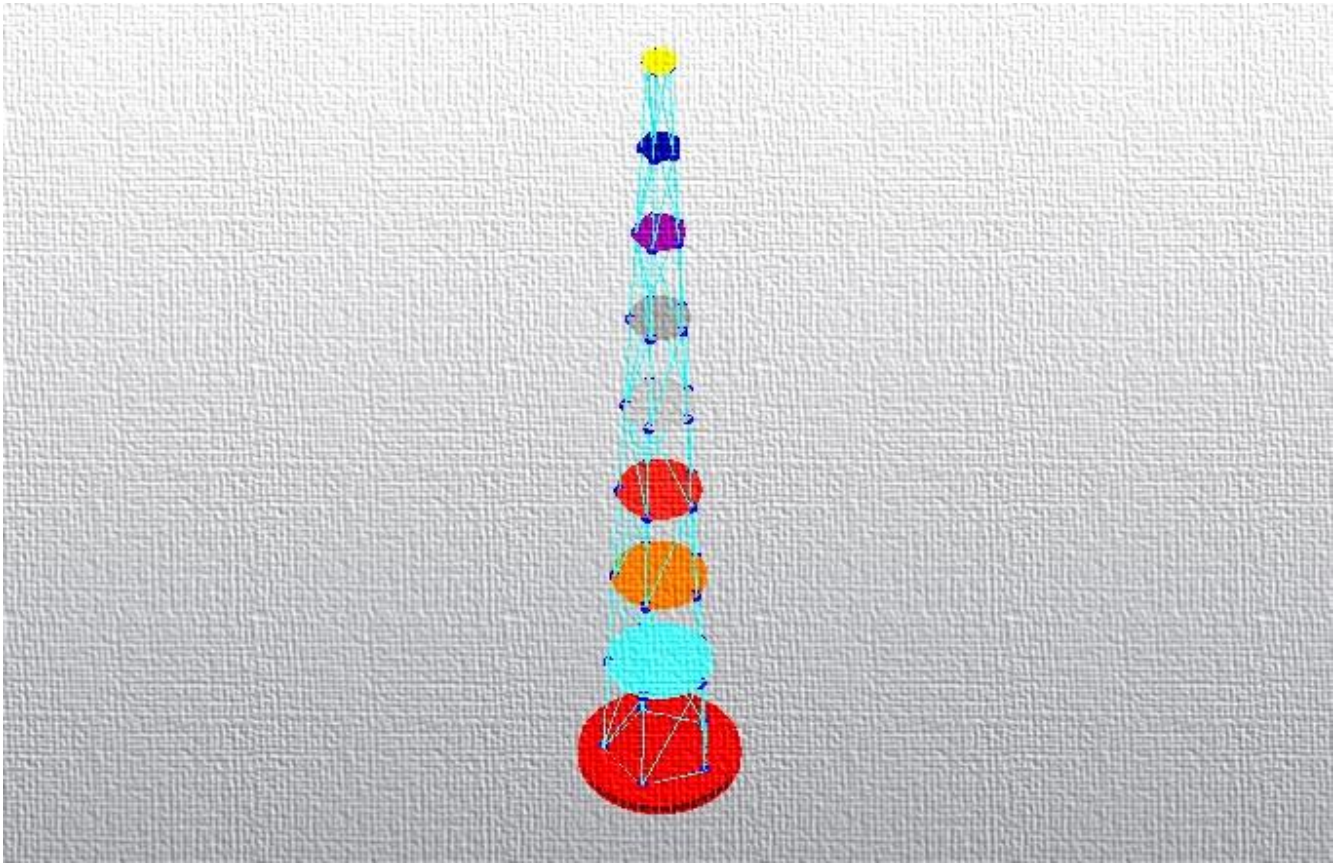

Conceptual design and FE analysis of a CLT wind turbine tower.

ALEJANDRO CANEL ÁLVAREZ, DARÍO CORTIZO FERNÁNDEZ

Department of Applied Mechanics
CHALMERS UNIVERSITY OF TECHNOLOGY
Gothenburg, Sweden 2016

Conceptual design and FE analysis of a CLT wind turbine tower.

ALEJANDRO CANEL ÁLVAREZ, DARÍO CORTIZO FERNÁNDEZ

Department of Applied Mechanics
Division of Material and Computational Mechanics
CHALMERS UNIVERSITY OF TECHNOLOGY
Göteborg, Sweden 2016

Conceptual design and FE analysis of a CLT wind turbine tower.
ALEJANDRO CANEL ÁLVAREZ, DARÍO CORTIZO FERNÁNDEZ

Master's Thesis 2016:21
ISSN 1652-8557
Department of Applied Mechanics
Division of Material and Computational Mechanics
Chalmers University of Technology
SE-412 96 Göteborg
Sweden
Telephone: + 46 (0)31-772 1000

Conceptual design and FE analysis of a CLT wind turbine tower.

ALEJANDRO CANEL ÁLVAREZ, DARÍO CORTIZO FERNÁNDEZ
Department of Applied Mechanics
Division of Material and Computational Mechanics
Chalmers University of Technology

Abstract

The conceptual design of a CLT (Cross Laminated Timber) wind turbine tower is presented in this thesis work. The proposed modular design is based on patent pending technology developed by Chalmers School of Entrepreneurship's startup Modvion. First, it is given a theoretical background about the employed wooden composite, the load state and further concerns. Then, the feasibility of building a self-supporting tower which fulfills a set of given requirements is discussed.
The composite tower has been modeled using the finite element method (FEM) to assess the uncertainties related to the idea. *Autodesk's Inventor 2016* and *Simulation Mechanical 2016* have been used for respectively modeling and performing FE analyses. Three criteria have been mainly employed for assessing the feasibility of the design: top deflection of the tower, failure index of the composite (according to Tsai-Wu's failure theory) and first eigenfrequency. Furthermore, a brief study comparing two different geometries for the cross-section of the tower is provided as well, as a special request by Modvion.
After this conceptual design stage, it was concluded that the given requirements could not be fulfilled without the usage of an external support structure e.g. a wire-based solution or an inner space frame truss. Possible alternatives based on such support structures are discussed and presented. A complete 3D model of the suggested tower is presented as well, including assembly instructions.
Finally, a brief discussion is used to sum up and conclude which aspects should be took into consideration for further optimization of the model.

Key words: Wind Turbine Tower Design, Wind Turbine Tower Load, Finite Element Analysis, Frequency Analysis, Cross Laminated Timber

Contents

Table of figures

Table of tables

Preface

This Thesis Work has been conducted from mid-January 2016 to early June 2016. The work is part of the developing process of a feasible wooden wind turbine tower design employing modular patent pending technology from Modvion. This company, framed in *Chalmers Ventures* programme, is a startup project willing to accomplish their objective of building their first wind turbine tower as the pinnacle of their business plan. The project is carried out at the Department of Applied Mechanics, Division of Materials and Computational Mechanics, Chalmers University of Technology, Sweden.

The work has been conducted with the inestimable help of Jim Brouzoulis as both advisor and examiner and Håkan Johansson as an advisor. Special thanks to Otto Lundman and Joakim Örneblad, the young visionaries behind Modvion, for believing in us as a team and keeping us busy with their requests and concerns. Thanks to David Olivegren as well, father of the original idea of the modular timber tower, always paying attention to the evolution of the project and proposing new solutions to those problems faced during the development of the Thesis Work.

We would also like to thank Reza Haghani Dogaheh for his unbelievable interest in the project despite his limited involvement. Your expertise and altruistic guidance through the ups and downs of the project has been highly appreciated.

Göteborg March 2016-01-01

ALEJANDRO CANEL ÁLVAREZ, DARÍO CORTIZO FERNÁNDEZ

Notations

Roman upper case letters

$C_{\mathrm{o}}(z)$	Orography factor
C_{pe}	External pressure coefficient
C_{p0}	External pressure coefficient without free-end flow
$C_{\mathrm{r}}(z)$	Roughness factor
D_{bottom}	Outer diameter at the bottom of the tower
$D_{\mathrm{bottom,inner}}$	Inner diameter at the bottom of the tower
D_{top}	Outer diameter at the top of the tower
$D_{\mathrm{top,inner}}$	Inner diameter at the top of the tower
E_{wire}	Young's modulus
$E_{0,\mathrm{mean}}$	Modulus of elasticity parallel to grain
$E_{90,\mathrm{mean}}$	Mean modulus of elasticity perpendicular to grain
E_1	Young's Modulus in the fiber direction
E_2	Young's Modulus in directions perpendicular to the fiber direction
F_{saf}	Factor of safety
F_{x}	along-wind force [N]
F_{y}	transverse-wind force [N]
F_{z}	turbine weight [N]
G_{mean}	Mean shear modulus
G_{12}	Shear modulus
H_{hub}	Hub height
I	Moment of inertia
$I_{\mathrm{v}}(z)$	Turbulence intensity at height z
K_{wire}	Stiffness of each cable
L_{wire}	Length of each cable
M_{x}	bending moment around X-axis [Nm]
M_{y}	bending moment around Y-axis [Nm]
M_{z}	torsional moment around Z-axis [Nm]
R_{m}	Tensile strength of the material (Pa) (see Table 5.4)
S	Cross-sectional area of a cable
S_t	Strouhal number (dimensionless parameter)
T	Cable tension (N)
T_{adm}	Maximum admissible tension in the wire (N)
T_{p}	Pretension in the wires (N)
$\mathrm{T_w}$	Increase in tension caused by the wind load (or any external action) (N)
V_{f}	Velocity factor. Ratio between the wind speed as a function of height and the basic wind speed
W	Mass of the weights placed on the surfaces (kg)

Roman lower case letters

c	Factor given by equation 5.10
c_{O}	Viscous damping coefficient
$f_{\mathrm{c,0,k}}$	Compression strength parallel to grain
$f_{\mathrm{m,k}}$	Bending strength

$f_{\mathrm{nat},i}$	Natural frequency of the considered flexural mode *i* of cross-wind vibration
$f_{\mathrm{t,0,k}}$	Tensile strength parallel to the grain
$f_{\mathrm{t,90,k}}$	Compression strength perpendicular to grain
$f_{\mathrm{v,k}}$	Shear strength
f_{vortex}	Frequency of vortex shedding
l_2	Distance between one end and the damping system as shown in Figure 5.14 (m)
m	Height between platforms. Constant value equal to **15 m**
m_{top}	Mass at the top of the tower (turbine system plus blades)
m_{tower}	Mass of the tower
n	Mode number
r	Ratio between the outer diameter of the tower at the bottom and at the top
r_{max}	Value of *r* that makes the inner diameter at the top equal to 3
r_{next}	Radius of the top platform in a certain level
r_{o}	Radius of the base platform in a certain level
$q_{\mathrm{p}}(z)$	Peak velocity pressure
$u(x_{\mathrm{O}})$	Displacement of the cable at the attachment (m)
v_{b}	Basic wind velocity at 10 m above ground level of terrain category II with an annual probability of exceedance equal to 0,02
v_{hub}	Wind speed at hub height
$v_{\mathrm{m}}(z)$	Mean wind velocity at a height z above terrain
w_{e}	External pressure
z	Height
z_{hub}	Hub height

Greek lower case letters

α	Inclination angle of the undeformed tower with respect to the vertical axis
α_{A}	Position of the flow separation
α_{min}	Position of the minimum value of the external pressure coefficient
α_{wire}	Inclination angle of each cable
γ	Elevation angle of the friction surface
γ_{12}	Shear strain
ε_1	Strain in the fiber direction
ε_2	Strain in directions perpendicular to the fiber direction
ζ	Damping coefficient achieved with the weights
λ	Factor given by equation 5.11
μ	Friction coefficient
μ_{wire}	Mass per unit length of the wire (kg/m)
ρ	Air density
ρ_{mean}	Mean density
ρ_{wire}	Mass density of the carbon fiber (kg/m^3)
σ_1	Stress in the fiber direction
σ_2	Stress in directions perpendicular to the fiber direction
τ_{12}	Shear stress
ν	Poisson's ratio
ω	Natural frequency of vibration of the cable

Greek upper case letters

ΔZ	Horizontal deviation at the height of the wire
Ψ	End-effect factor
$\Psi_{\gamma\alpha}$	End-effect factor

1 Introduction

Modvion is a startup project from Chalmers School of Entrepreneurship aiming to design - and eventually build - a modular wind power tower. The whole project is based on a patent pending technology regarding modular panels which may simplify transport issues, decrease manpower demands and on-site assembly time.

The core idea lies on designing a tower made out of cross-laminated timber (CLT) modules. The lower cost and lighter weight of the wooden-based material are the main advantages compared to traditional tower materials (such as steel and concrete).

1.1 Project goals

One overall aim of this project is to design the highest possible tower based on the aforementioned technology introduced in the patent. However, to be able to compare the developed concept with existing designs (using traditional materials) a height of 120 m was chosen as a suitable target. Therefore, the aim of the project is tightened to: develop a conceptual design of a 120 m wind tower in CLT.

To fulfill this goal the project has been structured into three different stages:

- Preliminary analysis: a simplified model of the tower will be adopted (where the tower will be considered homogenous and no attention will be payed to the joints). This study will serve as a feasibility test, in order to prove how reasonable the imposed requirements are. Obtained results will be used as the seed to carry out further in-depth analysis.
- As an extra request by Modvion, a geometry-based comparison study between an octagonal cross-section (concept of the main competitor) and a circular cross-section will be carried out.
- Final study: a final design of the outer structure, based on the modular assembly concept is proposed. Despite not having been considered as an initial goal, the outer structure of the tower will be supported by other systems so the height requirements can be finally accomplished.

1.2 Limitations, challenges and uncertainties

Despite some of the advantages of using CLT, many other aspects and properties make timber a less suitable material for building windmill towers when compared to steel and concrete, which are the most commonly employed materials nowadays. In addition, the innovation presented by the idea along with the uncertainties and lack of research related to the utilization of curved wooden materials (in terms of manufacturability and serviceability) introduces many unknowns in this project.
Several limitations have been imposed by the patent pending idea which are described in the following items:

- The tower should be made out of a pure timber-based composite material. This excludes any other potential material configurations, e.g. metal-timber composites) which minimizes the variety of feasible material-related alternatives that might solve certain issues.
- Modular design. The tower is built as an assembly of several pieces attached one to the other.
- The rounded-shaped cross-section places high demands on the manufacturing process due to the brittle nature of wood.
- The mechanism employed to attach the different modules is based on wooden rabbets and adhesive. Assembly issues can arise due to the large size of the glue lines imposed by the rabbets as well as the difficulties related to the curing process of the adhesive. Hence, mechanical fasteners might have to be employed.
- Moisture content affects strength and stiffness so it has to be properly addressed during the seasoning process. In this project, hygroscopic effects will not be considered since it is assumed that an outer layer of PVC will protect the tower by not letting the moisture in.
- Any kind of action coming from the ground will be considered negligible as explained in Section 3.
- The tower should be a self-supporting structure in accordance to the original idea conceived by Modvion in the patent, even though similar concepts (from competitors) have been built with the aid of an internal load-bearing structure. However, and since the ultimate goal of the project is obtaining a feasible solution, Modvion has been open minded regarding the possibility of including additional systems or equipment.

2 The composite material

2.1 Timber as structural material

Timber is one of the oldest materials known used in construction, as well as one of the most sustainable resources available nowadays. Timber transfers both tension and compression forces and possesses a high strength to weight ratio (specific stregth) and might be used as a suitable flexural member (primarily withstanding bending stresses). Wood structures can be repaired if damaged, thanks to how easily they can be reshaped or altered. Other inherent features are an impressive record for durability/performance and good insulating properties against heat and sound. All these characteristics make timber a material used in a wide variety of structural forms. In addition, centuries of experience of using timber as a construction material has helped to develop and understand safe methods of construction, suitable connection details and design limitations , cf. Porteous J., Kermani A. (2007).

Despite its extensive list of valuable properties, timber has many natural characteristics or defects which are introduced during the growth period and during the conversion and seasoning process. According to Porteous J. and Kermani A. (2007), all these issues have to be considered since they can reduce timber strength or impair its appearance. Some of them are listed below:

- Knots: their presence has negative effects on most mechanical properties by distorting the fibers around them, which leads to stress concentrations, or non-uniform stress distributions.
- Slope of grain: the deviation of the arrangement of fibers in wood with respect to the longitudinal axis affect certain properties such as bending strength or compression strength parallel to the grain.
- Reaction wood: it is referred to abnormal wood tissues produced in the tree trunks that are subjected to high wind pressures (this may cause the wood to fail in a brittle manner).
- Juvenile wood: it is the wood produced in the first rings of the trunk cross-section which exhibits lower strength and stiffness than the outer parts.
- Hygroscopic behavior: timber attempts to attain an equilibrium moisture content with its surrounding environment, resulting in a variable moisture content.

Wood is an anisotropic material; nevertheless, for structural purposes, it is assumed to be orthotropic (i.e. it is presumed to have directional properties in its three orthogonal axes) as is common. In Figure 2.1, the principal (orthogonal) axes are shown, being aligned with the grain direction (L), the tangential direction (T) and the radial direction (R).

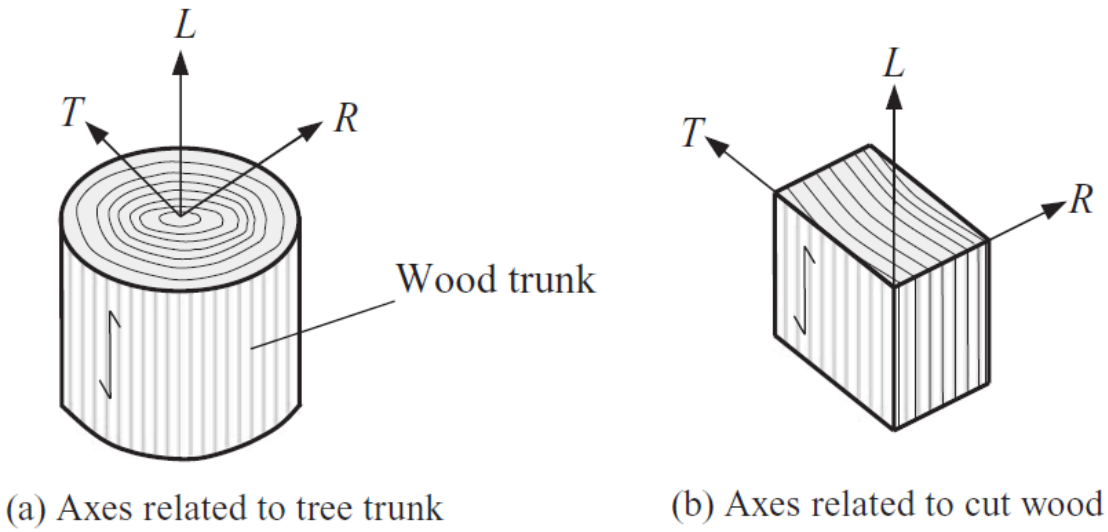

Figure 2.1 Principal axes of wood. Reproduced from: Structural timber design to Eurocode 5.

Properties parallel to the grain (L direction) are considerably stronger and stiffer than the corresponding properties along the R and T directions. Although the values of the respective properties in the R and T directions are not the same, the differences are small and for practical design purposes these properties are treated as equivalent. Properties in the R and T directions are referred to as properties perpendicular to the grain (Porteous J., Kermani A. [2007]). Consequently, timber will be characterized as what is known as a *transversely isotropic* material.

For a transversely isoelastic material, the constitutive law can be written as shown in equation (2.1) for the case of two-dimensional stress states (plane stress).

$$\begin{Bmatrix} \varepsilon_1 \\ \varepsilon_2 \\ \gamma_{12} \end{Bmatrix} = \begin{bmatrix} 1/E_1 & -\nu_{21}/E_2 & 0 \\ -\nu_{12}/E_2 & 1/E_2 & 0 \\ 0 & 0 & 1/G_{12} \end{bmatrix} \cdot \begin{Bmatrix} \sigma_1 \\ \sigma_2 \\ \tau_{12} \end{Bmatrix} \tag{2.1}$$

Where 1 and 2 refer to the fiber direction (grain direction L) and the transverse directions (R/T), respectively. σ and τ are normal and shear stresses, ε and γ are normal and shear strains, E is the Young's Modulus, ν is Poisson's ratio and G is the shear modulus.

Note that, there are five constants in equation (2.1). However; since the flexibility matrix is symmetric, only four of them are independent. Consequently only four matrix parameters are necessary to fully define the behavior of timber using this material model. It should be mentioned that the type of elements employed when creating the FE model are "thin composite" elements, which correspond to shell elements adapted to behave as the defined composite material.

2.2 Characteristic strength and stiffness properties of timber

Strength properties of timber are not easy to assess since, quite often, there is no control (e.g. monitoring, inspections, etc.) over its real quality and growth process. As stated in Section 2.1, several factors affect the strength; therefore strength grading methods are used to classify the timber. The way to determine design properties of timber might be either through non-destructive visual strength grading criteria or by machine strength grading (most common methods are either load- or deflection-controlled bending tests).
Grouping timber into strength classes was first introduced in the UK in standard BS 5268-2 in 1984. Nowadays BS EN 338:2003 defines 18 strength classes, including 12 for softwoods (C14, C16, C18, C20, C22, C24, C27, C30, C35, C40, C45 and C50) and 6 for hardwoods (D30, D35, D40, D50, D60 and D70). Compared to hardwoods, softwoods have a quicker growth rate (resulting in relatively low strength), poor durability qualities (unless treated) and are comparatively cheaper due to the speed of felling. This standard provides material property values for each strength class including:

- Bending strength [N/mm^2]: $f_{\mathrm{m,k}}$
- Tensile strength parallel (0) to the grain [N/mm^2]: $f_{\mathrm{t,0,k}}$
- Compression strength parallel (0) to grain [N/mm^2]: $f_{\mathrm{c,0,k}}$
- Shear strength [N/mm^2]: $f_{\mathrm{v,k}}$
- Compression strength perpendicular to grain [N/mm^2]: $f_{\mathrm{t,90,k}}$
- Modulus of elasticity parallel (0) to grain [kN/mm^2]: $E_{0,\mathrm{mean}}$
- Mean modulus of elasticity perpendicular (90) to grain [kN/mm^2]: $E_{90,\mathrm{mean}}$
- Mean shear modulus [kN/mm^2]: G_{mean}
- Mean density [kg/mm^3]: ρ_{mean}

2.3 Cross Laminated Timber (CLT)

Sawn sections of softwoods are limited in both quality and size. Any larger section than those available would suffer from defects caused by seasoning and conversion. In order to overcome those inherent limitations of sawn timbers, several Engineered Wood Products (also known as EWPs) have been developed throughout the years. These exist in a variety of forms and in combination with several adhesives. Some examples include: glulam, plywood or laminated veneer lumber.

CLT is a relatively new EWP with increasing usage as stated by Mohammad M., Gagnon S., K. Douglas B., Podesto L. (2012). In their own words "*[CLT] is a potentially cost competitive wood-based solution that complements the existing light frame and heavy timber options, and is a suitable candidate for some applications which currently use concrete, masonry and steel. CLT is an innovative wood product that was introduced in the early 1990s in Austria and Germany and has been gaining popularity in residential and non-residential applications in Europe. There are currently over one hundred CLT projects in Europe*".

Due to its relative youth, CLT has not been standardized and reference texts are scarce. There are four ongoing "efforts" regarding the standardization process of CLT products: i) European Draft; ii) FPInnovations drafts; iii) APA/ANSI PRG 320 Standard; iv) ISO Working draft. FPInnovations and their research group published a *CLT Handbook* (Gagnon S., Pirvu C. [2011]), peer-reviewed and widely used as a reference publication for CLT design. According to the handbook, CLT panels consist of several layers (at least three) of wood boards stacked crosswise (commonly at 90 degrees) and glued together either on their wide faces or sometimes in both wide and narrow faces. Figure 2.2 illustrates a CLT panel configuration.

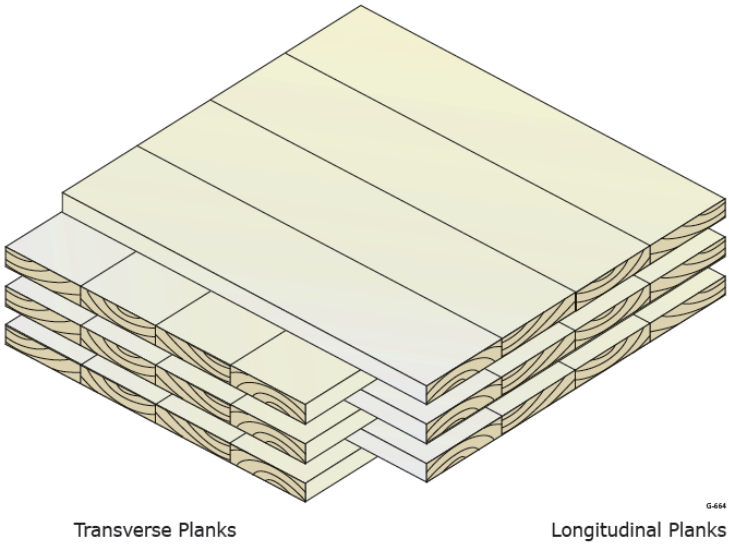

Figure 2.2 CLT panel configuration. Reproduced from: CLT Handbook.

The boards in the outer layers of the CLT panels acting as walls are commonly oriented parallel to the vertical loads that have to be withstood in order to maximize the wall resistance. This is because those outer plies are made out of wood from the highest strength class out of the two classes employed when manufacturing the composite-based modules (see Section 2.4 and stacking sequences presented in Table 4.1 Table 5.1).

2.4 CLT modules

The proposed tower will be designed using CLT modules made out of two different timber classes. These modules will be designed based on Modvion patent-pending original concept such they will fit together as a truncated cone puzzle (see Section 6 for the sake of clarification). Each module constitute what is called a laminated composite plate, or simply a laminate. These plates behave according to the properties of the transversely isotropic timber materials they are made of. Besides the inherent characteristics of the material of a certain layer, the behaviour of the laminate will be affected by the layup:

- Number of layers.
- Thickness of each layer.
- Orientation of each layer.

The structural response (stiffness) of the composite will be determined by the software itself based on the given material properties and the layup. The employed *Autodesk* (American engineering software corporation) software base their calculations on the Finite Element Method (FEM) using classical laminate theory.

Table 2.1 lists the strength and stiffness properties of the woods employed during the manufacturing process of the laminates (wooden modules). The right column refers to the properties of the timber used in those layers placed longitudinally whereas the left column makes reference to the properties of the transversely placed layers. Notice that longitudinal and transversal layers correspond to a certain extent to C14 and C24 strength classes as stated in BS EN 338:2003 (see Section 2.2).

Table 2.1 *Properties of the woods employed in the longitudinal/transversal layers of the laminated composite plate. Reproduced from: Handbok i KL-trä (by wood manufacturer Martinsons).*

Artikelnummer		**Tvärgående [N/nm²]**	**Längsgående [N/nm²]**
Karaktäristiska hållfasthetsvärden			
Bärhållfasthet	f m, k	14	24
Draghållfasthet			
- längsriktning	f t, 0, k	8	14
- tvärriktning	f t, 90, k	0,4	0,4
Tryckhållfasthet			
- längsriktning	f c, 0, k	16	21
- tvärriktning	f c, 90, k	2,0	2,5
- längsskjuvning	f v, k	3,0	4,0
- rullskjuvning	f R, k	1,0	
Styvheter för stabilitetsberäkningar			
Elasticitetsmodul	E 0,05	4700	7400
Styvheter för definitionsberäkningar			
Elasticitetsmodul	E 0, mean	7000	11000
	E 90, mean	230	370
Skjuvmodul	G mean	440	690
	G90, mean	50	50
Medelintensitet	p	~ 400 kg/m³	

2.5 Predicting failure in CLT

Failure will be assessed using *Tsai-Wu failure criterion*, which has been widely employed for anisotropic composite materials with different strengths in tension and compression.

Six failure criteria are representative of those that have been proposed over the years (Sun, C.T., Quinn, B.J., Tao, J. and Oplinger, D.W. [1996]). Failure criteria on the lamina level can be categorized into three groups:

- Limit criteria (maximum stress and maximum strain theories): the failure load and mode is predicted by comparing lamina stresses σ_{11}, σ_{22}, and τ_{12} (or strains ε_{11}, ε_{22}, and γ_{12}) with corresponding strengths separately. Interaction between the stresses or strains is not considered.

- Interactive criteria (Hill-Tsai and Tsai-Wu theories): the failure load is predicted by using a single quadratic or higher order polynomial equation involving all stress (or strain) components. Failure is assumed when the equation is satisfied. The mode of failure is determined indirectly by comparing the stress/strength ratios.

- Separate mode criteria (Hashin-Rotem and Hashin theories): these criteria separate the matrix failure criterion from the fiber failure criterion. The equations can be dependent on either one or more stress components; therefore, stress interaction varies from criterion to criterion within this group. If the failure equation contains only one stress component, then the failure mode corresponds to that particular direction; otherwise, the failure mode is determined by comparing stress/strength ratios.

Since Hill-Tsai and Tsai-Wu criteria include full stress interaction it seems reasonable to use either one or the other, even though maximum stress/strain criteria are still widely employed (see Figure 2.3).

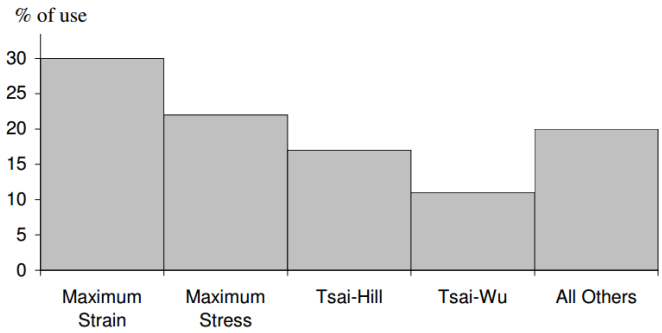

Figure 2.3 Industrial usage of composites failure criteria. Reproduced from: Failure criteria for fiber-reinforced composites.

Autodesk Simulation Mechanical 2016 (the main FE software used in this project) offers three failure criteria: maximum stress, maximum strain and Tsai-Wu. Hence, Tsai-Wu theory will be employed.

Tsai-Wu criterion calculates what is called the failure index, which predicts failure in a ply when the index reaches 1 or a higher value. Equation (2.2) expresses the failure criterion:

$$F_i\sigma_i + F_{ij}\sigma_i\sigma_j \leq 1 \tag{2.2}$$

Where F_i, F_{ij} are material parameters determined from the strength parameters stated in Section 2.2. σ_i, σ_j are the stresses $(i, j = 1 \dots 6)$ and correspond to Voigt notation as showed in equation (2.3):

$$\sigma = \begin{bmatrix} \sigma_{xx} & \sigma_{xy} & \sigma_{xz} \\ \sigma_{yx} & \sigma_{yy} & \sigma_{yz} \\ \sigma_{zx} & \sigma_{zy} & \sigma_{zz} \end{bmatrix} = \begin{bmatrix} \sigma_1 & \sigma_6 & \sigma_5 \\ \sigma_6 & \sigma_2 & \sigma_4 \\ \sigma_5 & \sigma_4 & \sigma_3 \end{bmatrix} \tag{2.3}$$

Rewriting the Tsai-Wu failure criterion for transversely isotropic materials gives equation (2.4):

$$F_2(\sigma_1 + \sigma_2) + F_3\sigma_3 + F_{22}({\sigma_1}^2 + {\sigma_2}^2) + F_{33}{\sigma_3}^2 + F_{44}({\sigma_4}^2 + {\sigma_5}^2) + F_{66}{\sigma_6}^2 + 2F_{12}\sigma_1\sigma_2 + 2F_{23}(\sigma_1 + \sigma_2)\sigma_3 \leq 1 \tag{2.4}$$

3 Boundary conditions

The tower is subjected to several loads caused by both external phenomena and disturbances imposed by the components which define the system. All boundary conditions can be classified as follows:

- Wind actions
- Loads caused by the turbine
- Foundation

The following sections describe the methodologies and criteria chosen to estimate the characteristic value of the above mentioned boundary conditions.

3.1 Wind loads

Wind actions are defined as so-called variable fixed actions as stipulated in EN 1991-4. Therefore, the fluctuating effect of wind action is simplified into a pressure gradient which varies as a function of height, acting on both the external and internal surfaces of the structure. The methodology suggested in EN 1991-1-4 has been followed in order to characterise a suitable wind profile for the conditions of the case study.

Wind actions give rise to forces and moments in the three dimensions. However, a simplified approach can be followed in accordance to S. Taranath, B. (2012) "*Wind buffeting against a bluff body is diverted in three mutually perpendicular directions, giving rise to these sets of forces and moments. […]. In civil engineering the force and moment corresponding to the vertical axis (lift and yawing moment) are of little importance. Therefore, aside from the effects of uplift forces on large roof areas, flow of wind is considered two-dimensional (2D), […], consisting of along wind and transverse wind*". Figure 3.1 displays an schematic model of this 2D wind actions.

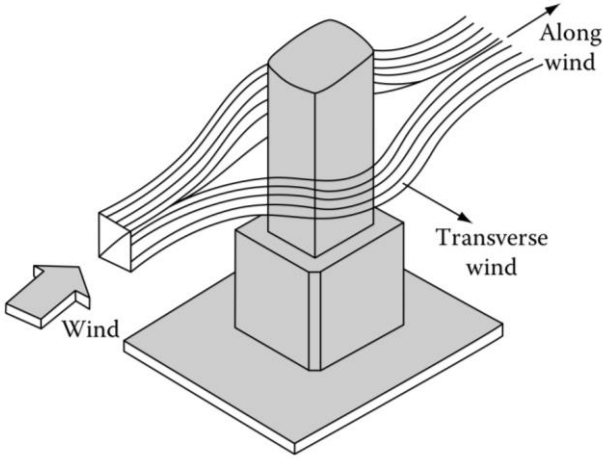

Figure 3.1 *Simplified 2D wind flow consisting of along-wind and across-wind. Reproduced from: Structural Analysis and Design of Tall Buildings: Steel and Composite.*

The wind pressure acting on the external surface of the tower is obtained from EN 1991-4 as:

$$w_e = q_p(z)C_{pe} \tag{3.1}$$

where:

w_e is the external pressure [Pa]
q_p (z) is the peak velocity pressure [Pa] (see Section 3.1.1)
z is the height from the ground [m]
C_{pe} is the pressure coefficient for the external pressure [-] (see Section 3.1.2)

Since the tower is an enclosed structure (covered at both ends) and the PVC coating applied to the external surface effectively reduces the porosity of the material, the internal wind pressure is neglected.

An overview of the procedure, as well as the assumptions, used defining the external pressure equations, are described in the subsequent sections.

3.1.1 Peak velocity pressure, $q_p(z)$

One model for the peak velocity pressure can be written as follows

$$q_p(z) = [1 + 7I_v(z)]\frac{1}{2}\rho v_m^2(z) \tag{3.2}$$

where:

ρ is the air density [kg/m^3] which has been chosen from ISO 2533 as a function of altitude, temperature and barometric pressure. The value chosen for this particular conditions (ground level and ambient temperature) is equal to 1,21933 kg/m^3.
$v_m(z)$ is the mean wind velocity at a height z above terrain [m/s]. Several factors regarding the terrain conditions need to be assumed in order to determine this parameter.

$$v_m(z) = C_r(z)C_o(z)v_b \tag{3.3}$$

where

v_b is the basic wind velocity at 10 m above ground level of terrain category II (as explained in the next paragraph) with an annual probability of exceedance equal to 0,02 (mean return period of 50 years). The reference wind speed for Gothenburg is quantified to a value of 25 m/s.
$C_r(z)$ is the roughness factor. It accounts for the change in the mean wind velocity due to the height above ground level and ground roughness of the terrain in the along-wind direction. In order to define this parameter, a theoretical location of the tower shall be imposed. Based on the common landscapes in Sweden, the description related to a category-II-terrain matches the requirements. "*Area with low vegetation such as grass and isolated*

obstacles (trees, buildings) with separations of at least 20 obstacle heights" as defined in the standard. Further information about the calculation of the roughness factor can be found in Section 8.

$C_o(z)$ is the orography factor. It accounts for the presence of hills, cliffs and/or other formations which alterate the flatness of the terrain and may increase wind velocities. Due to a lack of experimental data and uncertainties regarding the precise location of the tower, it is on the safe side to assume an orography factor equal to 1.

$I_v(z)$ is the turbulence intensity at height z. This parameter, in turn, depends on several factors such as the standard deviation, σ_v, turbulence factor, k_I and the roughness length, z_o. The latter acquires the value of 0,05 for a terrain category II. Once again, extensive calculation regarding the turbulence intensity can be found in Section 8.

3.1.2 Coefficient for the external pressure, C_{pe}

The external pressure coefficient is a dimensionless number representing the pressure distribution around the considered cross-section. This coefficient depends on two variables: the Reynolds number and the angle coordinate α relative to the wind velocity. Figure 3.2 shows the pressure distribution around a general cylinder along with the variation of the external coefficient with the Reynolds number and the angular position.

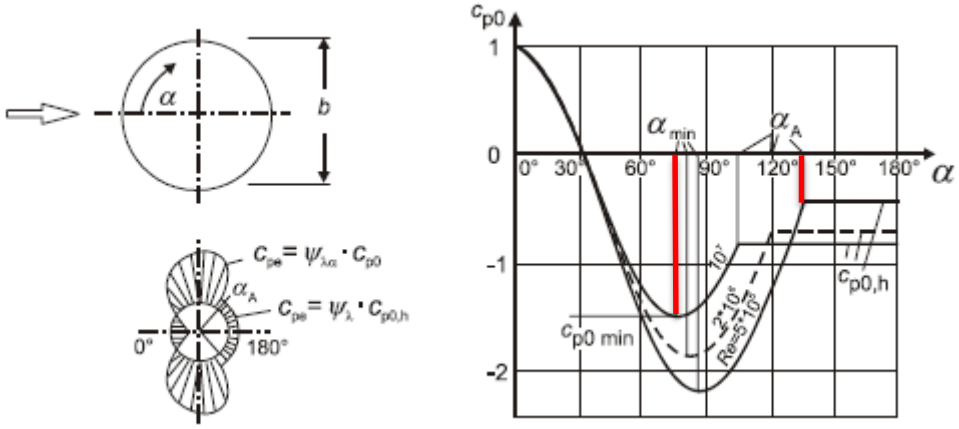

Figure 3.2 Pressure distribution for circular cylinders for different Reynolds number ranges and without end-effects. Reproduced from: EN 1991-1-4.

In order to consider end-effect factors (the end-effect factor accounts for the lower resistance of the structure due to the wind flow around the end), the general expression for the external coefficient is given as in EN 1991-1-4:

$$C_{pe} = C_{p0}\psi_{\gamma\alpha} \tag{3.4}$$

where:

C_{p0} is the external pressure coefficient without free-end flow

$\psi_{\gamma\alpha}$ is the end-effect factor. This parameter, in turn, depends on several factors submitted in the expressions below

$$\psi_{\gamma\alpha} = 1 \quad \text{for} \quad 0^{\circ} \leq \alpha \leq \alpha_{\min} \tag{3.5}$$

$$\psi_{\gamma\alpha} = \psi + (1-\psi)\cos\left(\frac{\pi}{2}\left(\frac{\alpha-\alpha_{\min}}{\alpha_{\mathrm{A}}-\alpha_{\min}}\right)\right) \quad \text{for} \quad \alpha_{\min} \leq \alpha \leq \alpha_{\mathrm{A}} \tag{3.6}$$

$$\psi_{\gamma\alpha} = \psi \quad \text{for} \quad \alpha_{\mathrm{A}} \leq \alpha \leq 180^{\circ} \tag{3.7}$$

where

$\alpha_{\min}, \alpha_{\mathrm{A}}$ are the angular positions shown in Figure 3.2.
Ψ is a factor which acquires a value equal to 0.75. Extensive information about the calculation of this coefficient is presented in Section 8.

In order to calculate a unique value of the external pressure coefficient in the wind-ward direction, an integration of the pressure distribution around the cross-section is required, projecting all vectors over the horizontal axis which gives

$$C_{\mathrm{pe}}(\alpha) = 2\int_{0}^{\alpha_{min}} \psi_{\gamma\alpha1} C_{\mathrm{p01}}(\alpha)\cos\alpha \, d\alpha \; + 2\int_{\alpha_{min}}^{\alpha_{A}} \psi_{\gamma\alpha2} C_{\mathrm{p02}}(\alpha)\cos\alpha \, d\alpha + 2\int_{\alpha_{A}}^{180} \psi_{\gamma\alpha3} C_{\mathrm{p03}}(\alpha)\cos\alpha \, d\alpha \tag{3.8}$$

Several assumptions and criteria have been adopted to solve the expression. All numerical values are taken from Figure 3.2:

- Reynolds number (defined as a function of the outer diameter, kinematic viscosity of air and peak wind velocity at hub height) for a 120 m tower (see parameters in *Table 4.3*) acquires a value around 10^7, thus the upper curve in Figure 3.2 is considered to model the equations for C_{p0}.
- Following the aforementioned criteria, $\alpha_{\min}$ and α_{A} adopt the values 75° and 105° respectively (see Figure 3.2, solid red lines).
- All the pressure vectors around the cross-section are pointing radially, hence they collide in the centre.
- The profile is considered independent of height (constant along the Z axis, in a normal orthogonal 3D coordinate system).
- Since the standard does not provide the explicit expressions for C_{p0}, an approximation using *Microsoft Excel* has been undertaken (approximation of upper curve in Figure 3.2). The result is three different curves ranging from 0° to 180°. Several points were selected from Figure 3.2 in order to obtain the expressions. The equations for each interval along with a graph displaying the selected curve (see Figure 3.3) are presented below.

$$C_{\mathrm{p01}} = 10^{-5}\alpha^3 - 0.0016\alpha^2 + 0.007\alpha + 1 \quad \text{for} \quad 0º \leq \alpha \leq \alpha_{\min} \tag{3.9}$$

$$C_{\mathrm{p02}} = 0.0008\alpha^3 - 0.128\alpha^2 + 3.4445 \quad \text{for} \quad \alpha_{\min} \leq \alpha \leq \alpha_{\mathrm{A}} \tag{3.10}$$

$$\mathrm{C_{p03}} = -0.8 \quad \text{for} \quad \alpha_{\mathrm{A}} \leq \alpha \leq 180^{\circ} \tag{3.11}$$

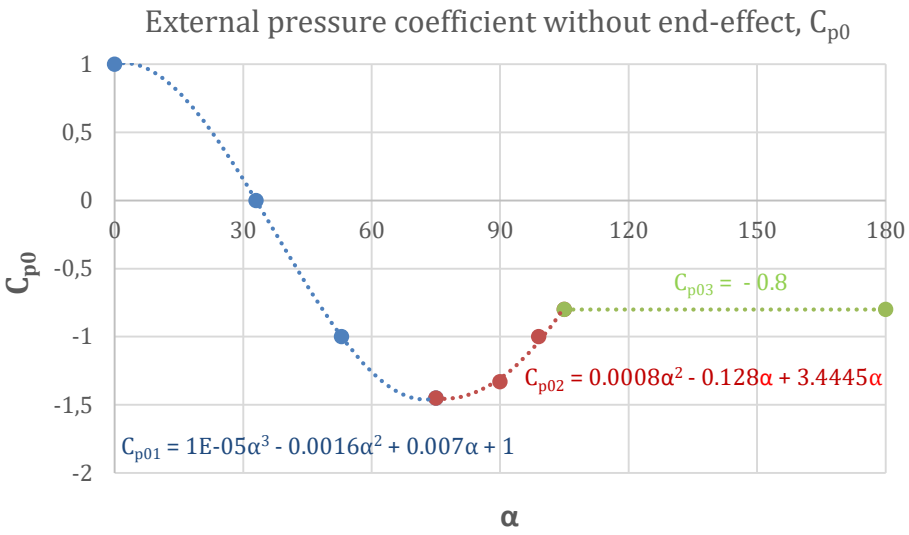

Figure 3.3 Pressure distribution approximation.

Substituting equations 3.9-3.11 and evaluating equation 3.8, results in a value for the external pressure coefficient $C_{\mathrm{pe}} = 3.1$. Further explanation of the method used to determine the coefficient is presented in Section 8.

3.1.3 Wind profile

Once the peak velocity pressure and the external pressure coefficient have been estimated, the last step lies in calculating the wind pressure profile along the height of the tower. Applying the expression for the pressure acting in the external surface (see Section 3.1, equation (3.1)), the wind profile can be plotted (as shown in Figure 3.4).

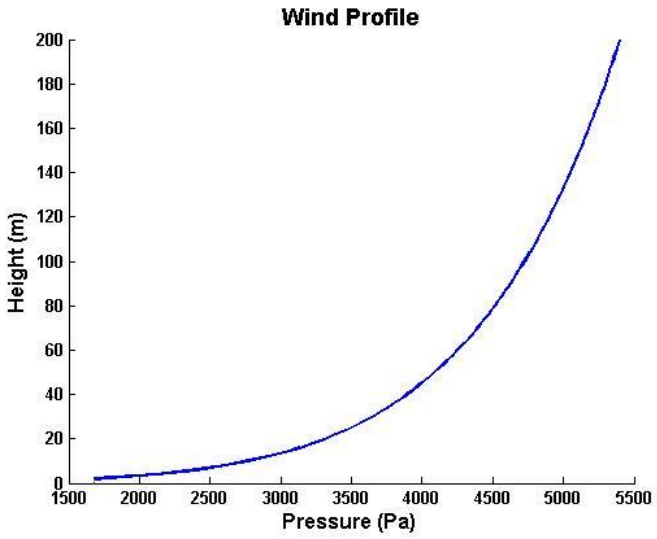

Figure 3.4 Wind pressure as a function of height.

3.2 Turbine disturbances

The placement of the turbine at the top of the tower inevitably imposes several effects in the structure. On one hand, the self-weight of both the rotor and generator substantially affects the natural frequency of the tower. On the other hand, the interaction between the turbine and wind loads results in several forces and moments that the tower must be able to withstand. The overall actions caused by the turbine are illustrated in Figure 3.5.

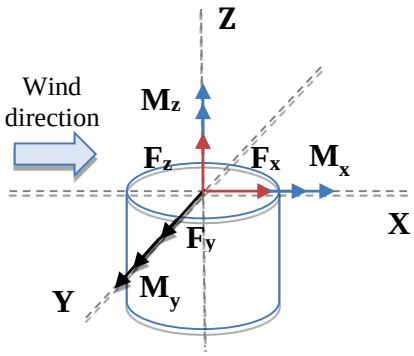

Figure 3.5 3D distribution of forces and moments resulting from turbine actions.

where

F_x along-wind force [N]
F_y transverse-wind force [N]
F_z turbine weight [N]
M_x bending moment around X-axis [Nm]
M_y bending moment around Y-axis [Nm]
M_z torsional moment around Z-axis [Nm]

The set of three forces and three moments is simplified down to two forces and two moments (F_x, M_x, F_z and M_z) for this case study. The force in the vertical direction constitutes the intrinsic weight of both the nacelle and rotor. As mentioned before, wind actions over the turbine result in a force in the along-wind direction, a bending moment around the Y-axis and a torsional moment around Z-axis.

Reference values have been assigned to the loads in order to analyse the tower response. In the case of the turbine mass, it is on the safe side to select the weight corresponding to the largest turbine. This will cause a large decrease in the natural frequency of the tower and may cause problems with vortex shedding, as explained in Section 3.4, and resonance as shown in Section 5.3. Regarding the along-wind force, F_x, bending moment, M_y, and torsional moment, M_z, the resulting increase in tower deflection and failure index only represents a small portion of the overall effect. Therefore, even though the actual values of the turbine (the model has not been selected in this preliminary stage) could differ from the ones assigned for this theoretical analysis, the ultimate impact of this variation in the tower is negligible. Table 3.1 describes and quantifies the different loads.

Table 3.1 Forces and moments values due to turbine actions

Loads (Unit)	Reference Value
Mass (kg)	350000
Along-wind force, F_x (kN)	810400
Bending moment, M_y (kN·m)	2500000
Torsional moment, M_z (kN·m)	-2727000

3.3 Foundation

The tower will be fixed to the ground by means of mechanical fasteners and/or other complementary structures. Several assumptions are considered for this part.

- The structure is perfectly fixed to the ground, thus no displacements nor rotations are allowed.
- Any kind of action coming from the ground is considered negligible (such as forces, seismic activity or vibrations).
- The material selected is fairly high strength concrete.

3.4 Vortex shedding

As stated in Section 3.1, wind flow effects might be considered to take place in two dimensions hence consisting of two components i.e. along wind and transverse wind.

The effect of transverse wind in the loading state of the tower is caused by a phenomena called *vortex shedding* or *Karman vortex* street. Generally, in tall building design, and even though the magnitude of drag forces caused by the along wind is more significant, the crosswind motion of the transverse wind is even more critical.

Figure 3.6 shows a prismatic building subjected to the effects of vortex shedding. The originally parallel upwind streamlines are displaced on either side of the building. At low wind velocities, the vortices are shed symmetrically in pairs, one from each side. When vortices are shed, a load is applied in the transverse direction. However, since the shedding occurs at the same time on either side of the building, there is no tendency for the building to vibrate in the transverse direction.

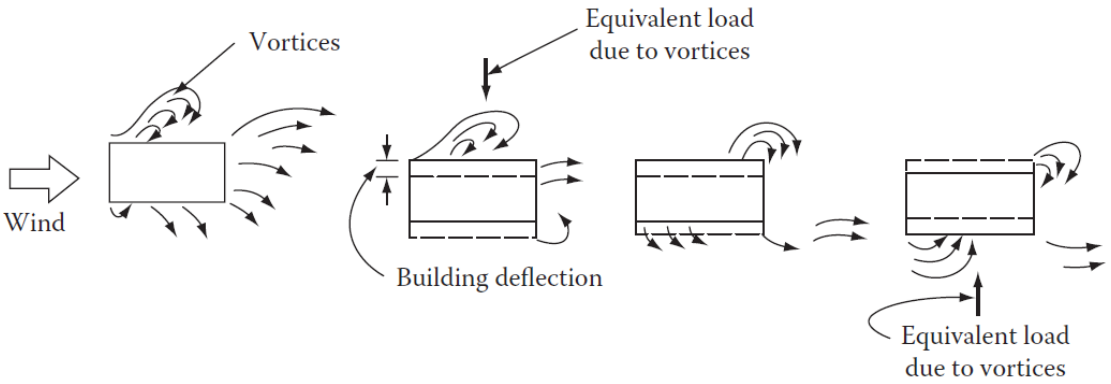

Figure 3.6 *Vortex shedding: Periodic shedding of vertices generates building vibrations transverse to the direction of the wind. Reproduced from: Structural Analysis and Design of Tall Buildings: Steel and Composite Construction.*

A different scenario is developed at higher wind speeds, when vortices are shed alternately from one side to the other causing an impulse in the transverse direction. This impulse due to transverse shedding generates vibrations in the transverse direction. It is therefore critical for the tower designer to assure that the natural frequency of the tower is above that value, in order to avoid resonance effects. A simple formula to estimate the frequency of the transverse pulsating forces caused by vortex shedding is shown in equation (3.12):

$$f_{vortex} = \frac{v_m \cdot St}{D_{top}} \tag{3.12}$$

where:

f_{vortex} is the frequency of vortex shedding in [Hz]
v_m is the mean wind speed at the top of the tower [m/s]
St is the Strouhal number (dimensionless parameter)
D_{top} is the outer diameter at the top of the tower [m]

The Strouhal number may be taken from *Table E.1* in BS EN 1991-1-4:2005 (Eurocode 1), which is 0.18 for rounded cross-sections.

It is interesting to notice that *"after the structure has begun to resonate, further increases in wind speed by a few percent will not change the shedding frequency, because the shedding is now controlled by the natural frequency of the structure. The vortex-shedding frequency has, so to speak, locked in with the building natural frequency"* (S. Taranath, B. [2012]). The importance of avoiding resonance is thus highlighted by this fact.

According to BS EN 1991-1-4:2005, Annex E, the effect of vortex shedding can be avoided by assuming a 25% security margin with respect to the natural frequency of the considered flexural mode. Therefore, in order to avoid resonance caused by vortex shedding, the following equation must be fulfilled:

$$f_{nat,i} \geq 1.25\, f_{vortex} = 1.25 \frac{v_m \cdot St}{D_{top}} \tag{3.13}$$

Where $f_{\mathrm{nat},i}$ is the natural frequency of the considered flexural mode i of cross-wind vibration.

4 Preliminary study

This section presents the results from a preliminary study concerning two main goals:

- Checking whether building a self-supporting 120 m outer structure of a wind turbine tower is feasible or not (by determining the deflection, failure index and natural frequency in order to confirm the need of an inner structure and/or other mechanism).
- In case a self-supporting 120 m tower is not viable, estimating how high the self-supporting tower can be and which the needed dimensions to build the outer structure are (checking that those conceptual towers are between the limits of feasibility in terms of deflection, failure index and natural frequency).

For that purpose, and as it can be noticed in the above paragraph, three output values determine the feasibility of the tower design:

- Deflection at the top of the tower: any deflection must be below 1.25% of the tower hub height.
- Failure index: as described in Section 2.5, a failure index above 1 will be translated into the failure of the timber composite.
- Natural frequency: the natural frequency of the tower must be above the vortex shedding frequency and out of the range of the frequency of the rotational speed of the turbine and its blades in order to avoid resonance.

All these parameters are computed by the FE software.

4.1 The FE model

In the preliminary study, a simplified version of the outer structure of the wind turbine tower was used. This simplified model considers the tower as a whole neglecting the effects of the joints, fasteners and adhesives. Figure 4.1 shows the simplified tower modelled in *Autodesk Inventor Professional 2016*. Notice that the outer shape of the model is a truncated cone.

Hereafter, variables that define the geometry of the tower are listed together with reference values of the boundaries.

- $\boldsymbol{D_{\mathrm{bottom}}}$: is the outer diameter at the bottom of the tower. $D_{\mathrm{bottom}}[m] \in [8\,,15]$.
- $\boldsymbol{t} = \frac{(D_{\mathrm{bottom}} - D_{\mathrm{bottom,inner}})}{2} = \frac{(D_{\mathrm{top}} - D_{\mathrm{top,inner}})}{2}$: is the thickness of the wall (and thus the thickness of the laminated composite plates). t [mm] ≤ 500 mm due to manufacturing limitations.
- $\boldsymbol{r} = {D_{\mathrm{bottom}}}/{D_{\mathrm{top}}}$: is the ratio between the outer diameter of the tower at the bottom and at the top. $r \in [1, r_{\mathrm{max}}]$ where r_{max} is the value of r that makes the inner diameter at the top equal to 3 i.e. $D_{\mathrm{top,inner}} \geq 3$ due to inner space needs (i.e. maintenance tasks, elevator, extra equipment...).
- $\boldsymbol{H_{\mathrm{hub}}}$**:** is the hub height of the tower. Its target value is 120 m.

Figure 4.1 Simplified model of the tower used during the preliminary study.

The simplified model is imported to *Autodesk Simulation Mechanical 2016* in order to perform "static stress with linear material models" and a "natural frequency (modal)" analysis.

In all of the analyses carried out during this preliminary study phase, the composite laminate stacking sequence has been the same (see Table 4.1 for a description of the used stacking sequence).

Table 4.1 Laminate stacking sequence used during the preliminary study phase (part 1 of 2).

Layer No.	Thickness [m]	Orientation angle [°]	Material
1	0.05	0	C24
2	0.02	45	C14
3	0.02	-45	C14
4	0.05	0	C24
5	0.02	45	C14
6	0.02	-45	C14
7	0.05	0	C24
8	0.02	45	C14
9	0.02	-45	C14
10	0.05	0	C24
11	0.02	45	C14
12	0.02	-45	C14
13	0.05	0	C24

Table 4.2 Laminate stacking sequence used during the preliminary study phase (part 2 of 2).

Layer No.	Thickness [m]	Orientation angle [°]	Material
14	0.02	45	C14
15	0.02	-45	C14
16	0.05	0	C24

Where layer no. 1 is the innermost ply whereas layer no. 16 is the outermost ply.

The motivation for choosing the layup presented in Table 4.1 comes from the following requirements:

- Total thickness of the laminated composite plate is the maximum i.e. 500 mm.
- The thickness of each longitudinal ply doesn't exceed the 60 mm upper boundary imposed by the manufacturer.
- The thickness of each transverse ply doesn't e the 20 mm upper boundary imposed by the manufacturer.
- Longitudinal plies (i.e. those with an orientation angle equal to 0) are slightly thicker than transversal layers. Longitudinally placed layers are oriented parallel to the vertical loads that have to be withstood in order to maximize the wall resistance. On top of that, longitudinal plies are made out of the timber of the highest strength class among the two employed i.e. C24.
- Transversal layers have an orientation of +45° and -45° alternatively. This orientation has proven to be the best in order to lower the failure index, although a lower deflection is obtained when reducing the angle, i.e. orienting transversal plies as if they were longitudinal.

The layout concept has been directly taken from the patent. Further modifications will be performed during the in-depth analysis phase.

4.2 Self-supporting 120 m tower

The 3D model of the tower has been subjected to the loads and boundary conditions as described in Section 3. Parameters related to the geometry have been determined in order to minimize deflection and failure index (see Table 4.3).

Table 4.3 Geometric parameters of the 120 m tower model employed in the preliminary study phase.

Parameter	Unit	Value
D_{bottom}	m	15
r	-	3.75
t	mm	500
H_{hub}	m	120
D_{top}	m	4
α	°	2.62

Where α is the inclination angle of the undeformed tower with respect to the vertical calculated according to equation (4.1):

$$\alpha = atan\left(\frac{D_{bottom}-D_{top}}{2H_{hub}}\right) \tag{4.1}$$

Figure 4.2 and Figure 4.3 show the response of the tower to the applied load state.

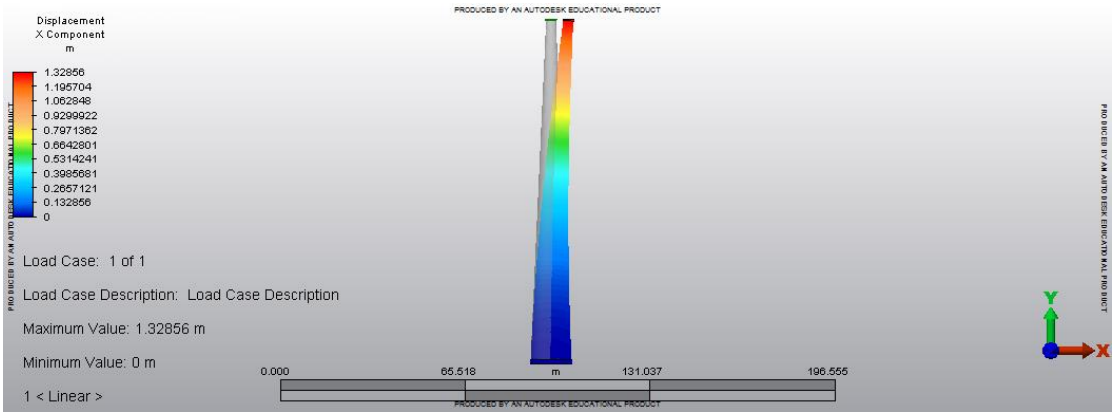

Figure 4.2 Displacement (X component) of the 120 m tower preliminary model.

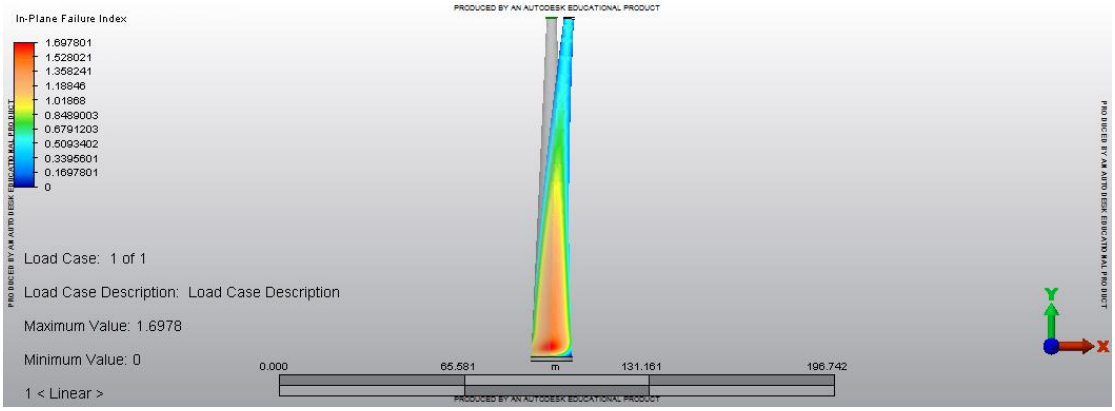

Figure 4.3 Failure index of the 120 m tower preliminary model.

Even though the deflection at the top of the tower is admissible (1.3286 m ≤ $0.0125H_{\text{hub}}$), the failure index remains above 1 at certain spots and layers of the tower, which means that the timber would eventually fail. Rotation due to torsional loads at the top of the tower remains below 0.2°, which is far from being considered a problem.

Regarding the modal analysis, Table 4.4 lists the first 5 of the frequencies for the first 5 modes of vibration.

In accordance to equation (3.13), $f_{\text{vortex}} = 1.6637$ Hz and thus $f_{nat,i} < 1.25\ f_{\text{vortex}}$ when $i = 1{,}2$. This means that the tower may experience resonance problems caused by the vortex shedding.

In this preliminary study, no inner structures or other stiffening systems are considered; therefore a 120 m target height seems unfulfillable.

Table 4.4 First 5 eigenfrequencies of the 120 m tower preliminary model.

	[Hz]
$f_{\text{nat},1}$	0.3935
$f_{\text{nat},2}$	0.3938
$f_{\text{nat},3}$	2.7475
$f_{\text{nat},4}$	2.7483
$f_{\text{nat},5}$	5.9723

4.3 Self-supporting feasible towers

Based on the results presented in Section 4.2, a self-supporting 120 m tower is not considered feasible in terms of failure index and resonance risk. Lower towers might be feasible in terms of failure index, however because of the slender design and inherent properties of timber materials, fulfilling the requirements related to the natural frequency of the tower is difficult without increasing certain parameters beyond the boundaries stablished in Section 4.1. On top of that, height is considered a critical parameter, hence decreasing it far below 120 m would be seen as a failure.

For the purpose of assessing which variables should be modified in order to improve the response of the tower against vibrations caused by the passing blades (see Section 5.3) and vortex shedding, it is presented an expression of the natural frequency of the first bending mode for a beam fixed at one end with a constant cross section and a mass at the other end (D. Blevins, R. [2001]):

$$f_{nat,1} \approx \frac{1}{2\pi}\sqrt{\frac{3EI}{{H_{hub}}^3(m_{top}+0.24m_{tower})}} \tag{4.2}$$

Where E is the Young's Modulus of the tower, I is the moment of inertia and m_{top} and m_{tower} are respectively the mass of the turbine+blades and the mass of the tower.

Note that equation (4.2) is only a rough estimate since the cross section of the employed 3D model is not constant. According to the expression, in order to increase the natural frequency of the tower, several parameters can be modified. Nevertheless, height—which highly affects the result— and Young's modulus, cannot be modified as freely as desired since the tower has to be built out of timber and the height should be kept as large as possible.

Because of the impossibility of fulfilling frequency-related goals —while analyzing the self-supporting structure alone— without unfulfilling the rest of the requirements, frequency issues will be neglected in this section. Dampening systems and/or any other way of mitigating resonance should be studied further, otherwise the design would be unsatisfactory.

Hundreds of analyses have been carried out modifying the geometric parameters introduced in Section 4.1. Figure 4.4 to Figure 4.7 show different feasible models in terms of deflection and failure index. D_{bottom} has been kept as low as possible

within the boundaries described in Section 4.1. Their natural frequencies of the first bending mode remain low, hence equation (3.13) is not fulfilled in any of these models.

Notice that the models shown from Figure 4.4 to Figure 4.7 simply aim to illustrate how feasible self-supporting solutions with different heights may look and how the parameters that define these models need to be changed in order to achieve feasibility when the height is increased. The last (and highest) of the presented models (Figure 4.7) represent the tallest self-supporting tower that would stand by itself. This means that regardless of the change of the geometric parameters described in Section 4.1 (as long as the defined boundaries are met), there is no feasible tower taller than 90 m (90 to 94 m, since analyses were carried out varying height with a span of 5 meters).

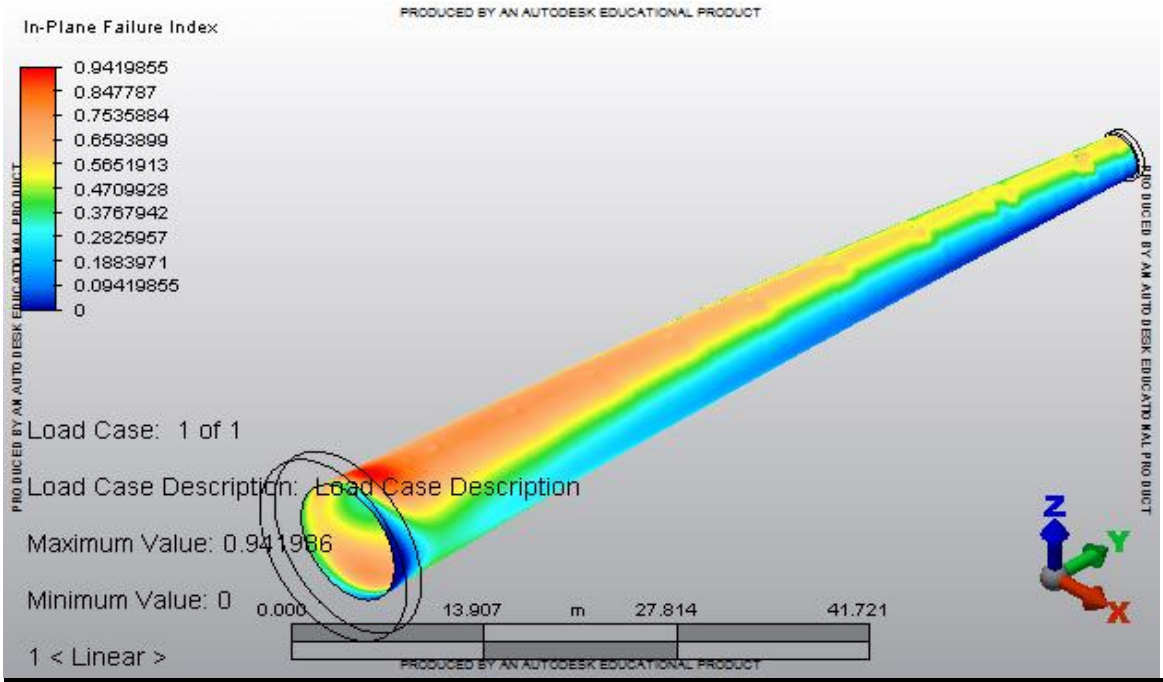

D_{bottom} [m]	r	t [m]	H_{hub} [m]	D_{top} [m]	α [m]	Max. deflection [m]	Max. failure index	$f_{nat,1}$ [Hz]
10	2.5	0.5	75	4	2.291	0.553	0.942	0.487

Figure 4.4 Feasible 75 m tower.

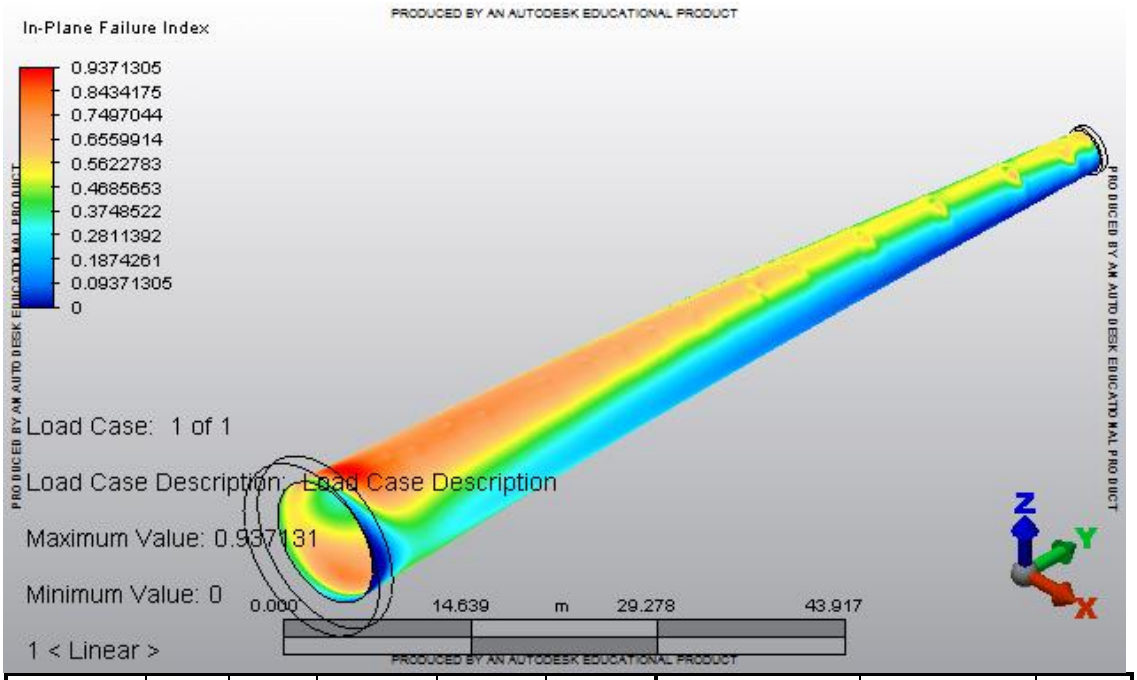

D_{bottom} [m]	r	t [m]	H_{hub} [m]	D_{top} [m]	α [m]	Max. deflection [m]	Max. failure index	$f_{nat,1}$ [Hz]
11	2.75	0.5	80	4	2.505	0.567	0.937	0.497

Figure 4.5 Feasible 80 m tower.

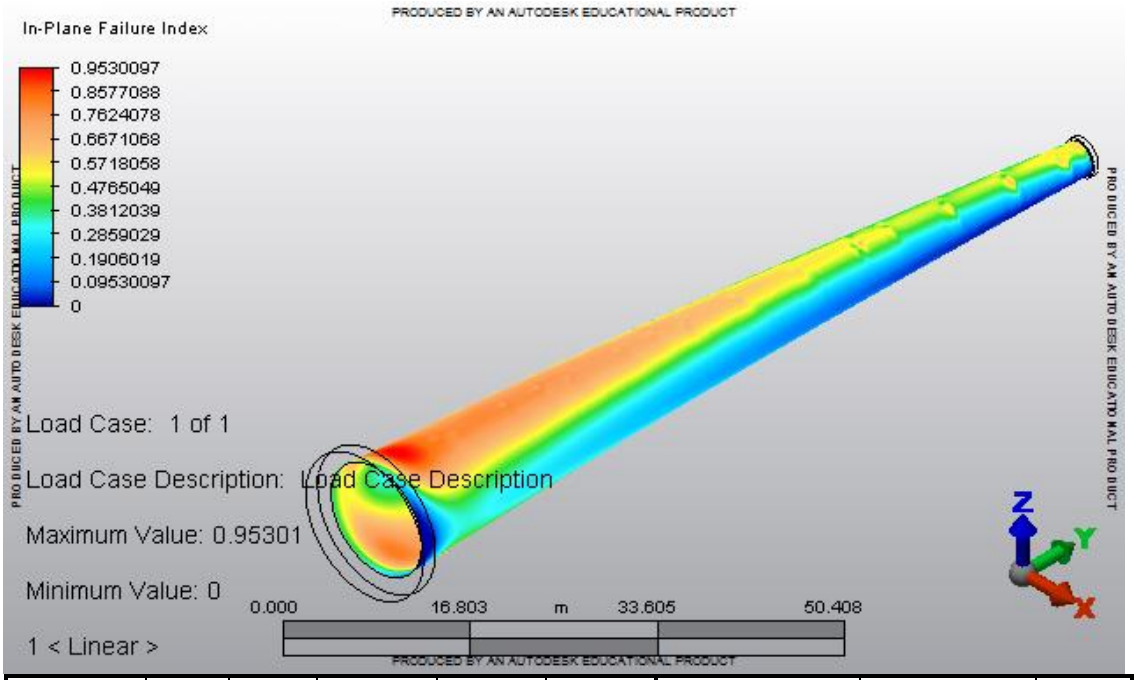

D_{bottom} [m]	r	t [m]	H_{hub} [m]	D_{top} [m]	α [m]	Max. deflection [m]	Max. failure index	$f_{nat,1}$ [Hz]
12	3	0.5	85	4	2.694	0.585	0.953	0.504

Figure 4.6 Feasible 85 m tower.

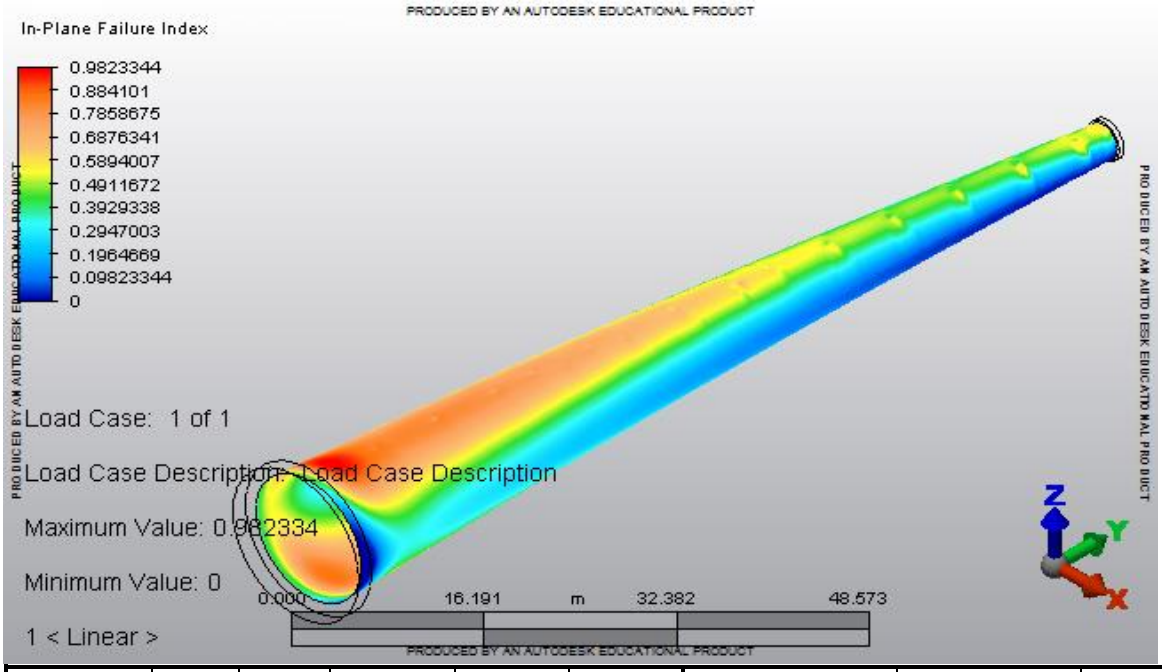

D_{bottom} [m]	r	t [m]	H_{hub} [m]	D_{top} [m]	α [m]	Max. deflection [m]	Max. failure index	$f_{nat,1}$ [Hz]
13	3.25	0.5	90	4	2.862	0.607	0.982	0.509

Figure 4.7 Feasible 90 m tower.

4.4 Circular and octagonal cross-section. Geometrical comparison

In order to investigate some of the differences between the concepts proposed by the main competitor's design and the studied one, a comparison between the octagonal (competitor's design) and circular cross-sections (case study) have been carried out. The aim of this extensive review is to study the behaviour of the tower when it is subjected to a static wind load and all the actions from the turbine as well as the distribution of pressures created around the external surface due to the wind action.

Two different analysis have been undertaken to accomplish the aforementioned aspects:

- A wind tunnel simulation, using *Autodesk Robot Structural Analysis* 2016, has been employed to compute pressure contours around both external surfaces. The main purpose of such simulation is to analyse how the wind adapts to both geometries and the loads created around the cross-sectional areas in order to determine which is the optimal shape.
- A static linear analysis, using *Autodesk Simulation Mechanical* 2016, has been implemented to attain the tower response in both scenarios.

4.4.1 Wind tunnel simulation

The software includes a wind simulation feature that allows the application of wind flows to a structure in order to obtain results to either visualize pressure contours or compute wind loads.

Certain inputs needs to be fixed to define the wind scenario, in order to obtain reliable results, as well as the CAD models:

- Since the external geometry of the structures is the main part of this analysis, the CAD models have been kept simple. Therefore, both an octagonal prism and a circular cylinder have been extruded setting the dimensions given in Table 4.5 .
- Wind speed. It is fixed at a value equal to the basic wind speed, v_b (see Section 3.1.1)
- Wind direction. Since the models are completely symmetric around the X and Y-axis, the simulations are carried out with a constant wind direction as shown in Figure 4.8. Selecting different wind directions (in the check boxes shown in Figure 4.8) leads to more simulations (in case two directions are checked, two independent simulations are carried out for each model). However, since the models are symmetric, the outcome from such simulations would be the same, or highly similar, hence a constant wind direction is considered sufficiently accurate.
- A new wind velocity profile has been implemented by compliance with the rules specified in IEC 61400-1. The shape of the profile is given by the power law exposed below.

$$v(z) = v_{hub}\left(\frac{z}{z_{hub}}\right)^{0,2} \tag{4.3}$$

$$V_f = \frac{v(z)}{v_b} \tag{4.4}$$

Where:

v_{hub} is the wind speed at hub height. 50 m/s is considered an appropiate maximum value.
z_{hub} is the hub height.
V_f is the velocity factor. Ratio between the wind speed as a function of height and the basic wind speed, v_b.

- Terrain level where the structure is placed. It is considered a value of **0 m** for both cases.

Figure 4.9 shows the final wind profile once the inputs and variables explained in the bullet list have been applied.

Table 4.6 CAD model main dimensions. Reproduced from: http://www.timbertower.de/products/

Height (m)	Outer Diameter (m)	Thickness (m)
100	7	0,3

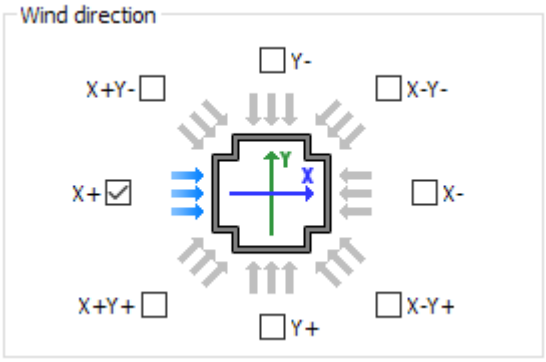

Figure 4.8 *Wind directions selected for the simulations. Reproduced from: Autodesk Robot Structural Analysis 2016.*

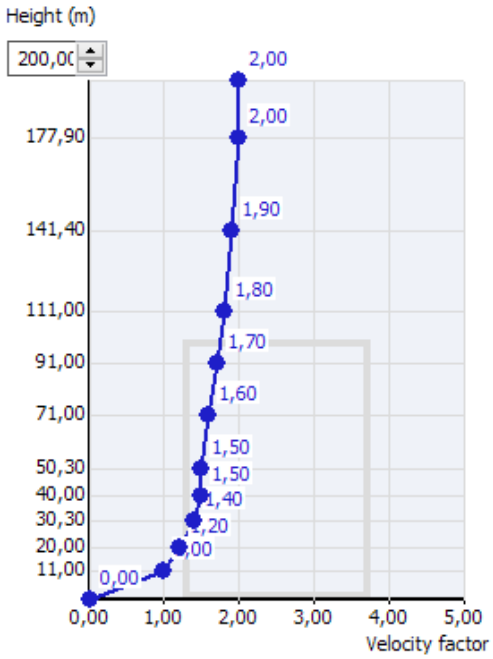

Figure 4.9 *Wind profile shape implemented in the software.*

As the next step, an in-depth description of the results computed with the software is presented. The following set of images displays the resulting pressure contours for both the octagonal and circular 3D geometries when the wind is blowing in the X+ direction as well as the loads generated around the top cross-section of each tower.

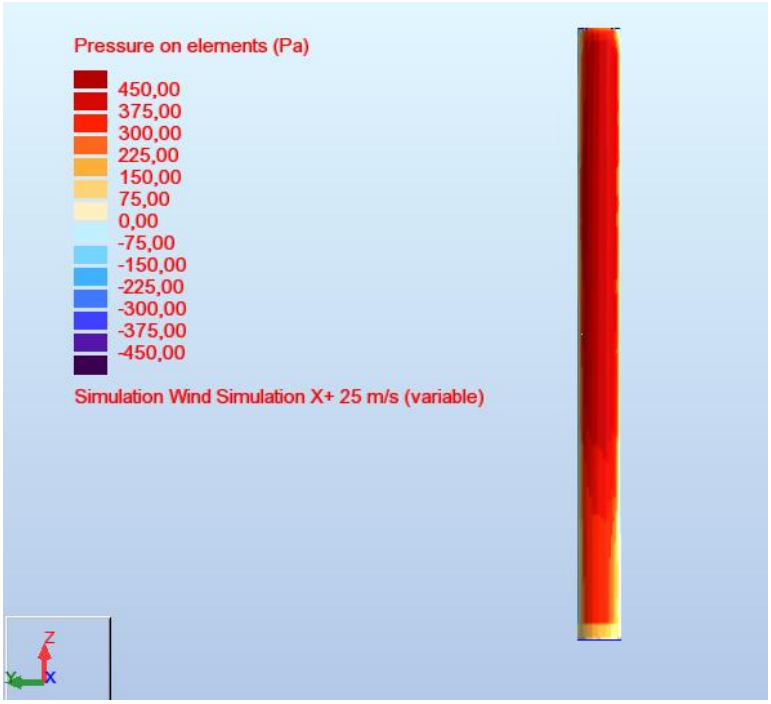

Figure 4.10 Front view of the pressure contour for the circular tower.

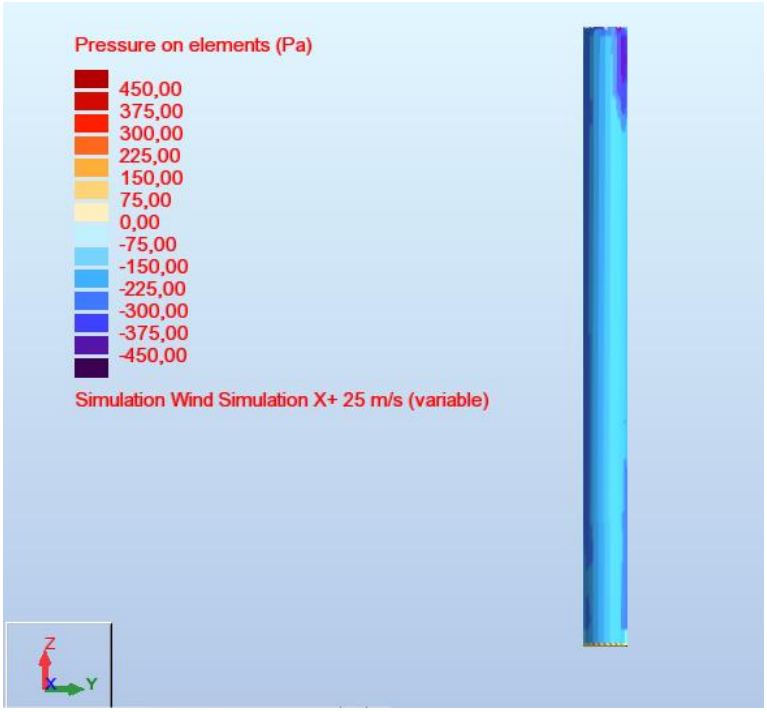

Figure 4.11 Rear view of the pressure contour for the circular tower.

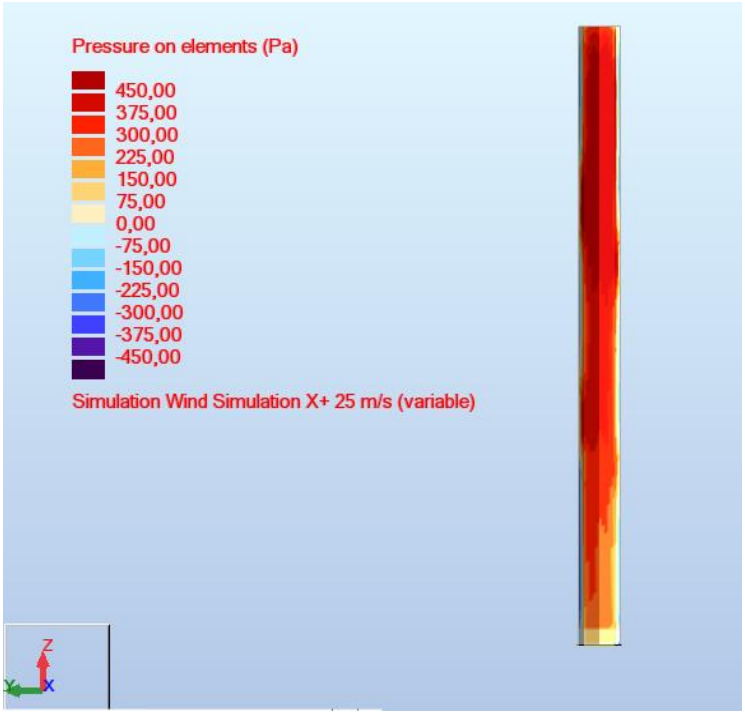

Figure 4.12 Front view of the pressure contour for the octagonal tower.

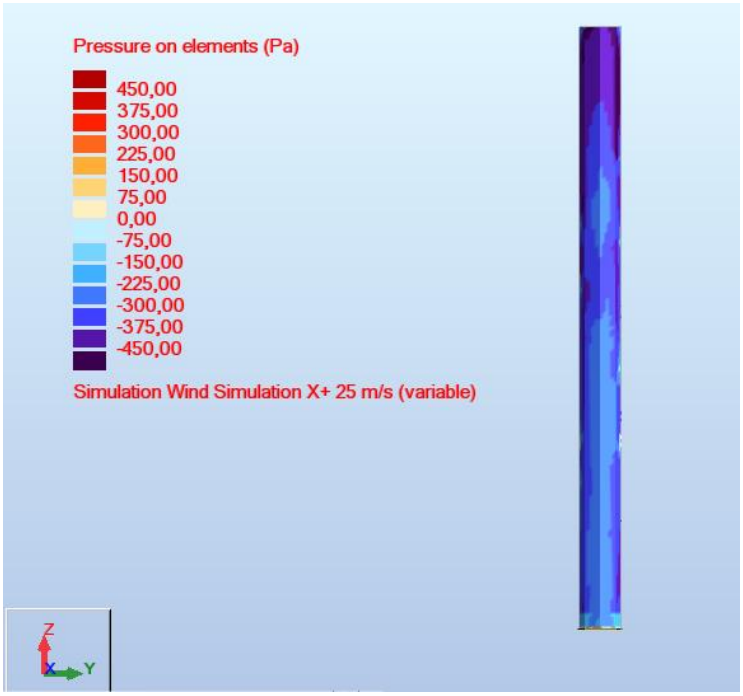

Figure 4.13 Rear view of the pressure contour for the octagonal tower.

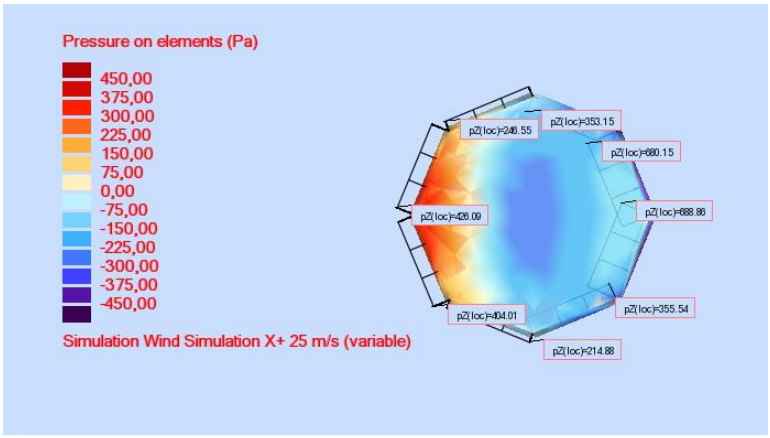

Figure 4.14 Loads generated on top of the octagonal tower due to wind flow.

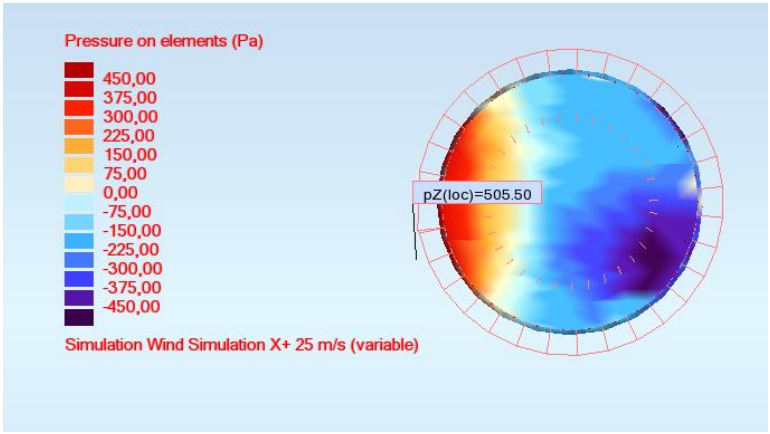

Figure 4.15 Loads generated on top of the circular tower due to wind flow.

Several conclusion can be derived from the previous figures:

- Due to the similarities between an octogonal and a circular shape, as well as the slenderness of the structure (low ratio of transversal over longitudinal dimension), the surface pressure shows a similar distribution pattern in both models. Nevertheless, a more even and homogeneus pressure distribution is obtained by the circular cross-section, with smoother pressure profiles, mostly in the rear part of the structure where lower negative pressures are induced relative to the polygonal shape.
- Regarding the loads generated due to the wind flow, it is noticeable the uneven distribution around the octogonal cross-section (see Figure 4.14), in contrast to the even distribution achieved with the circular shape. This phenomenon might lead to stress concentracion on the edges as well as deformation of the polygonal cross-section. To sum up this point, a circular shape will withstand radially-oriented loads of equal magnitude, therefore it might be less stressful for the structure given the symmetrical pattern of the loads.

4.4.2 Static linear analysis

The static analysis aims to compare the deflection undergone by the structure and the failure index in the different layers when both towers are subjected to the loads described in Sections 3.1-3. For this particular analysis, more detailed models were used considering that the structure is tapered. The dimensions and properties of the new models are given in Table 4.7.

Table 4.7 Ratio bottom/top diameter, material and number of layers of the towers

Height (m)	Outer Bottom Diameter (m)	Thickness (m)	r	Material	Number of layers
100	7	0.3	2.42	C14, C24	16

The main dimensions of the tower were selected based on the specification given by the competitor's design (height, thickness, base diameter and ratio bottom/top diameter). However, the lack of information in regards to the material type and number of layers in the conforming plates required assumptions to be made, the used layup shown in Table 4.7.

The following figures show the maximum deflection of the tower as well as the failure index in the most stressed layer for both cases.

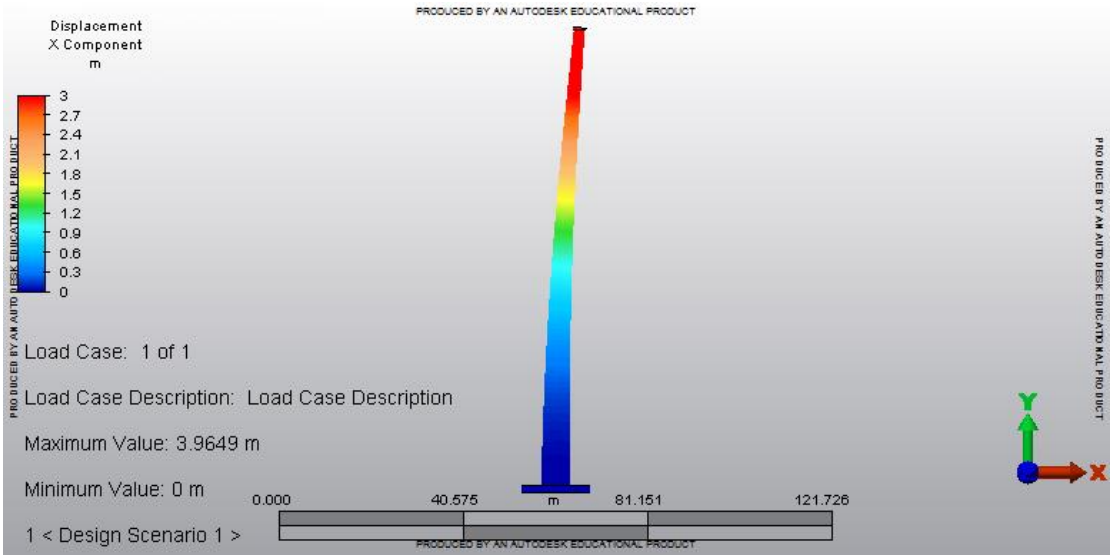

Figure 4.16 Horizontal displacement distribution experienced by the rounded tower.

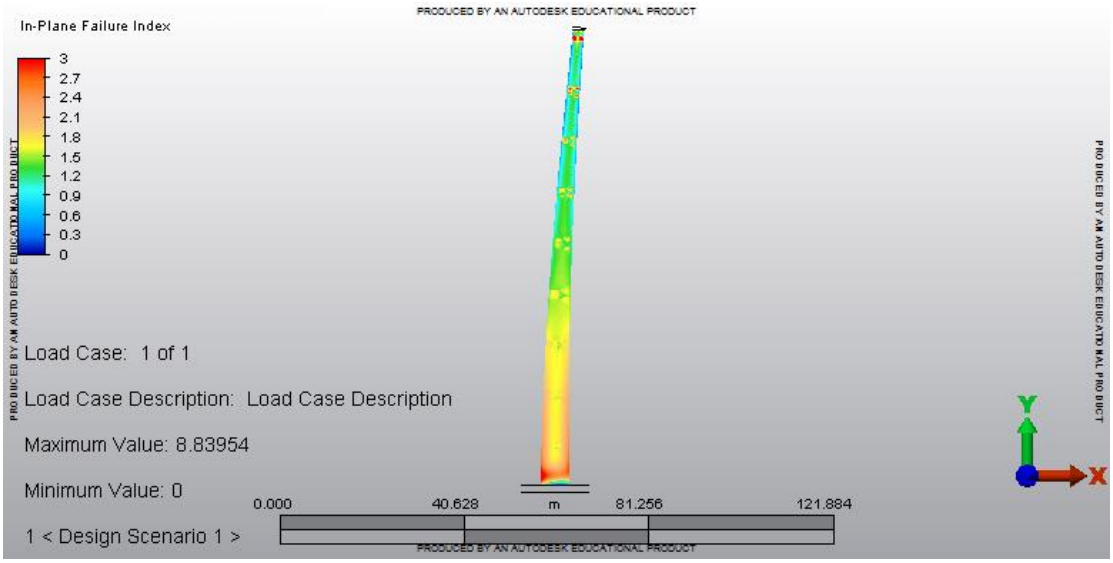

Figure 4.17 Failure index distribution experienced by the rounded tower.

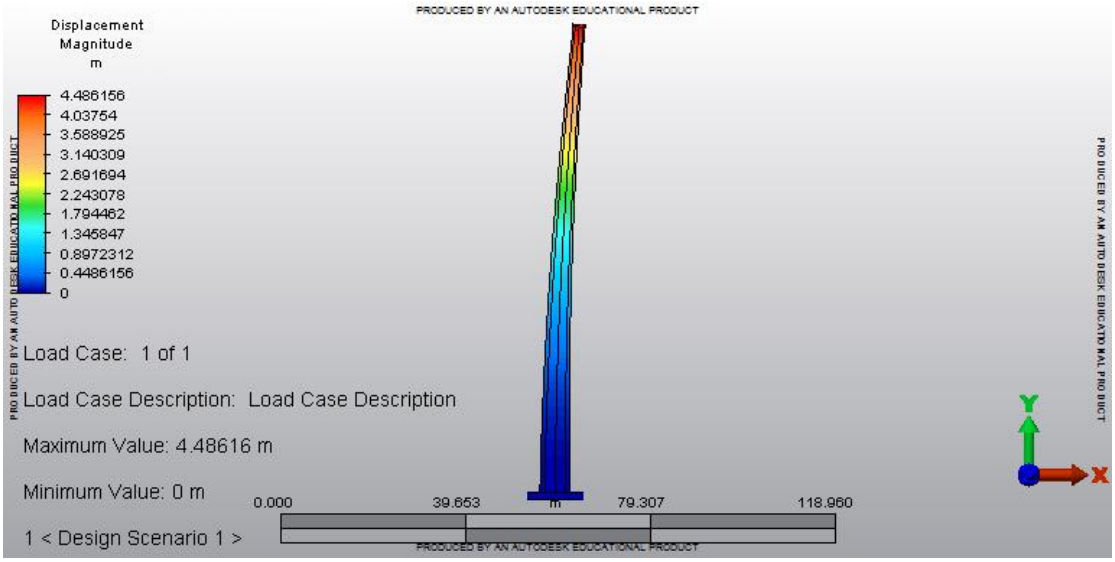

Figure 4.18 Horizontal displacement distribution experienced by the octagonal tower.

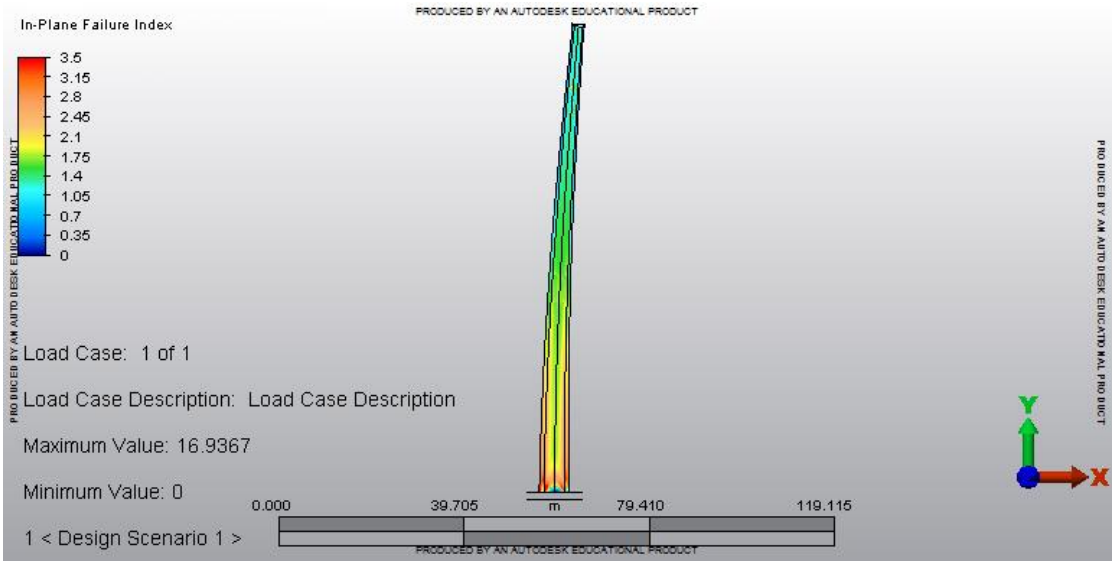

Figure 4.19 Failure index distribution experienced by the octagonal tower.

The figures clearly show larger deflection for the octagonal tower when subjected to the loads. The polygonal structure undergoes a deflection 13 % higher than the displacement presented with the rounded shape. Furthermore, the maximum failure index experienced by the outer layers goes up to 17, as opposed to the highest value displayed by the circular tower, which is slighly below 9.

One explanation of the different performances lies on the smoother and continous layout proposed by the circular shape, as opposed to the more agressive lines which characterise any polygonal section. The sharp edges presented by the octagonal cross-section lead to higher values of the failure index on the vicinity of the connections between faces.

However, this analysis should be carefully interpreted. The software applies certain simplifications which can lead to uncertainties in the results. For starters, when meshing the rounded tower, the program considers a perfectly uniform shell with no divisions, as opposed to the actual model (connections between modules). In addition, the wind load will vary very much in time and from one structure to the other as it is affected by the geometry of the structure (for this analysis the same wind load have been applied in both models).

Therefore, in order to obtain a more reliable solution, an in-depth analysis (focusing on a minor scale such as carrying out a thorough study of the connections between modules) and/or load tests should be carried out.

The closure of the current section gives way to the final study phase. The following sections present solutions for the achivement of a 120 m tower as it was adressed in Section 1.

5 Final study

Up to this point, a few feasible self-supporting designs have been proposed (see Section 4.3). However, the ultimate goal of obtaining a feasible 120 m tower hasn't been fulfilled yet. Section 5 explores solutions beyond the self-supporting concept in order to achieve a feasible solution, neglecting the self-supporting nature requirement.

Several aspects of the design and loads have been modified in this new iteration of the project with the clear target of obtaining a 120 m feasible design:

- Due to manufacturing issues, the laminate stacking sequence has been altered compared to the one presented in Table 4.1. The resulting sequence is shown in Table 5.1. Notice that the imposed requirements regarding the stacking sequence (see Section 4.1) are still fulfilled in this new one.
- The top mass (which corresponds to the weight of both the nacelle and the rotor) has been lowered since the chosen value during the preliminary study was too high (selected on purpose on the safety side). The new value will be 150 tons, which seems to be a more realistic approach according to turbine manufacturers and the expertise of the advisors for this project.
- The usage of an external support system (aside of the tower structure itself) to modify the first natural frequency of the tower. The main effort is focused on adding cables or an internal space truss as a supporting structure.
- Internal platforms every 15 m of height need to be installed. Those are not expected to substantially improve the performance of the tower, however since they are necessary for maintenance purposes, they will be implemented.
- Strength/stiffness-related properties of wood will be affected by the moisture content. Therefore, a protective PVC outer layer is planned to be installed, not letting moisture in, hence avoiding the aforementioned problem.

Table 5.1 Laminate stacking sequence used during the final study phase (part 1 of 2).

Layer No.	Thickness [m]	Orientation angle [°]	Material
1	0.045	0	C24
2	0.02	45	C14
3	0.045	0	C24
4	0.02	-45	C14
5	0.045	0	C24
6	0.02	45	C14
7	0.045	0	C24
8	0.02	-45	C14
9	0.045	0	C24
10	0.02	45	C14
11	0.045	0	C24

Table 5.2 Laminate stacking sequence used during the final study phase (part 2 of 2).

12	0.02	-45	C14
13	0.045	0	C24
14	0.02	45	C14
15	0.045	0	C24

Notice that the geometric parameters related to the 120 m self-supporting tower are the same as those shown in Table 4.3.

5.1 Tower design with modified stacking sequence and reduced top mass

The new stacking sequence, c.f. Table 5.1, alternates a longitudinal layer and a transverse one, in contrast to the previous stacking sequence, c.f. Table 4.1, where two transversal layers were consecutively placed in between two longitudinal plies.

Figure 5.1 and Figure 5.2 show top deflection and failure index for the 120 m tower but with the new stacking sequence and the reduced mass of 150 t on top.

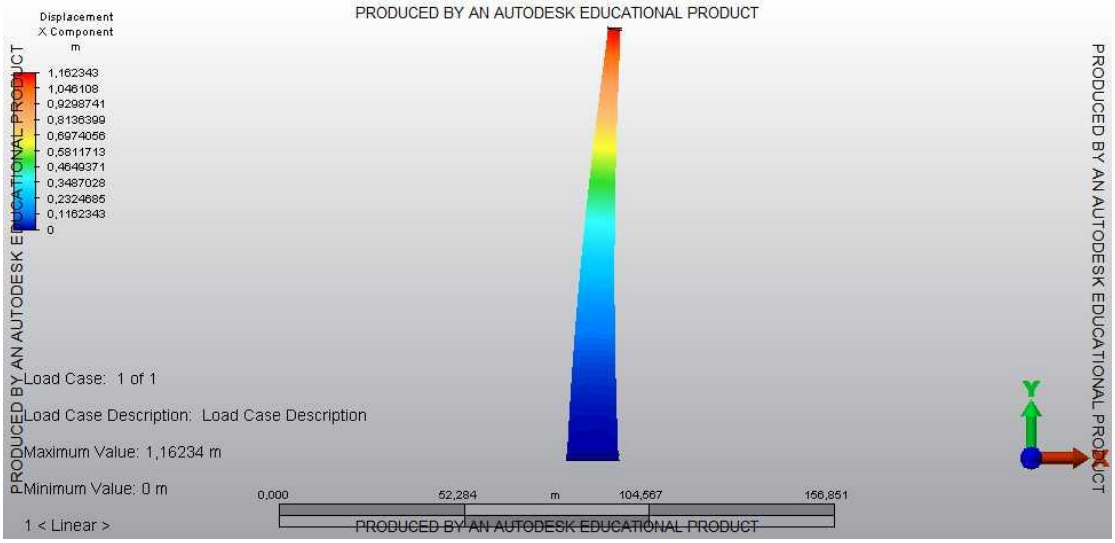

Figure 5.1 Deflection of the 120 m tower with the new stacking sequence and the 150 t mass on top.

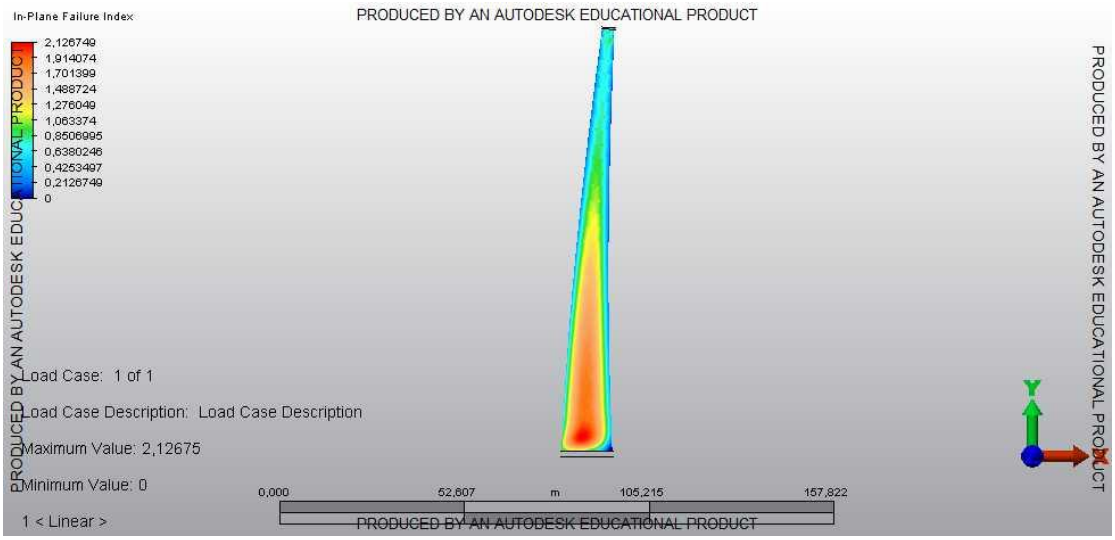

Figure 5.2 Failure index of the 120 m tower with the new stacking sequence and the 150 t mass on top.

Compared to the results obtained in Section 4.2 using the old stacking sequence (and with a 350 t mass on top), the new sequence reveals new top deflection, failure index and $f_{nat,1}$ values (see Table 5.3).

Table 5.3 Comparison between the 120 m tower with the previous and the new stacking sequence.

	Top deflection [m]	**Failure Index**	**$f_{nat,1}$ [Hz]**
Old stacking sequence	1.3286	1.6978	0.3935
New stacking sequence	1.1623	2.1267	0.5522

The new stacking sequence affects the failure index negatively, whereas the new lower top mass decreases the top deflection and increases the value of $f_{nat,1}$.

5.2 Inner platforms

Once the new stacking sequence had been implemented, a comparison between the tower with and without the inner platforms was carried out. Figure 5.3 shows how the seven platforms ((7+1) platforms * 15 m/platform = 120 m) have been added into the model:

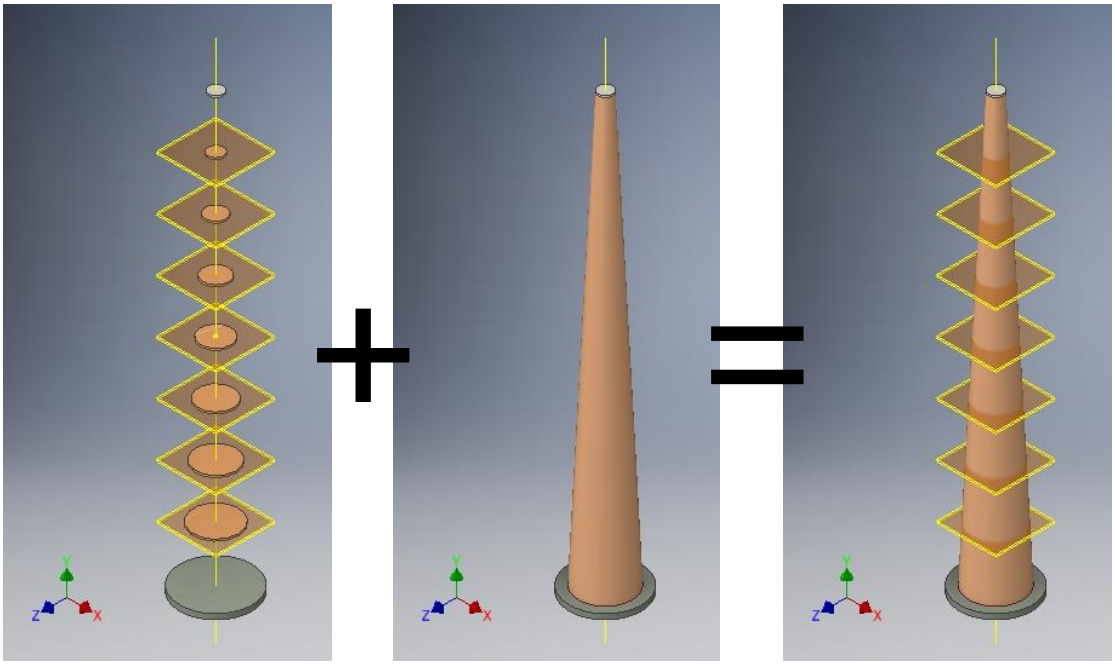

Figure 5.3 Implementation of the inner platforms.

Figure 5.4 and Figure 5.5 show that there is almost no improvement, once the inner platforms are considered, compared to having no platforms (Figure 5.1 and Figure 5.2). Both, top deflection and failure index keep their value close to those showed in Section 5.1.

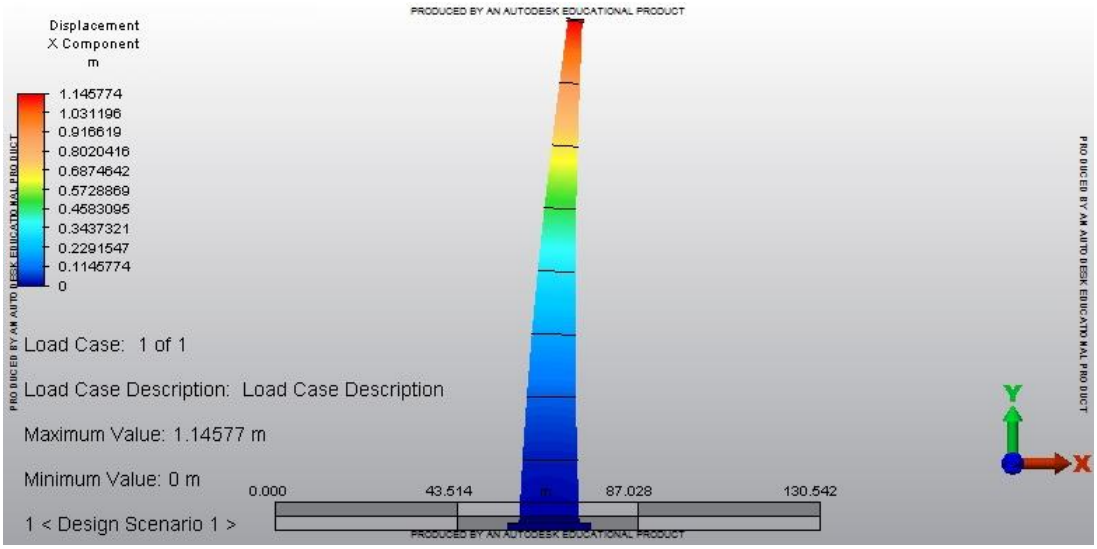

Figure 5.4 Top deflection of the 120 m tower with the platforms.

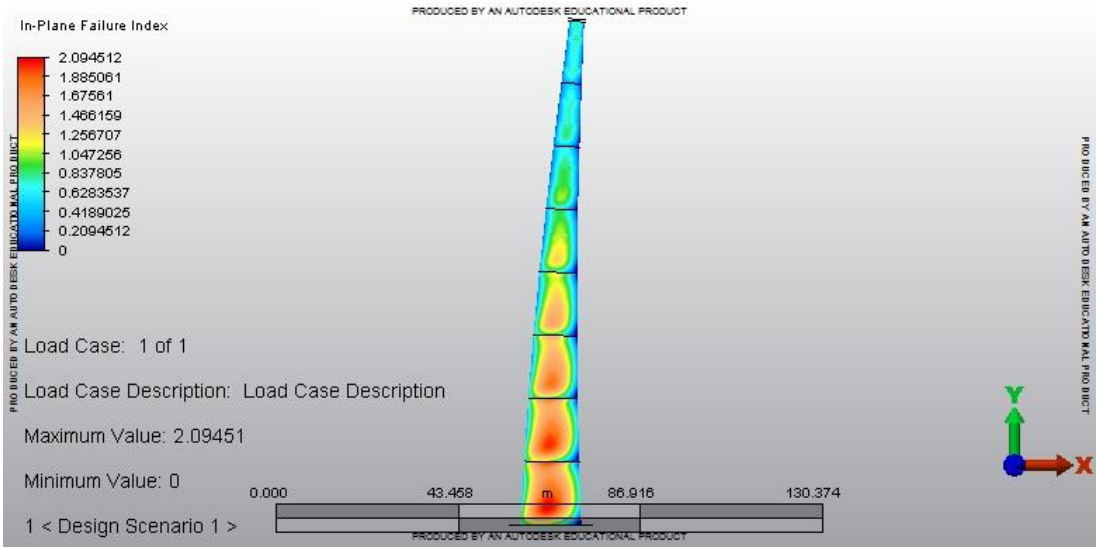

Figure 5.5 Failure index of the 120 m tower with the platforms.

The addition of weight caused by the 7 wooden platforms (0.5 m thickness) decreases the value of $f_{nat,1}$ from 0.5522 to 0.5481 Hz. Steel platforms might lower the frequency towards 0.4672 Hz due to its higher density.

5.3 Eigenfrequency strategy

A wind turbine tower can be categorized into three different classes depending on where its natural frequency lies with respect to the operational range. Prior to making this classification, the frequency range where the turbine will operate needs to be determined.

The main source of dynamic loads are imbalance in the shaft and/or rotor and aerodynamic loads of passing blades. The rotational speed of the blade, N, as well as three times this value (three blades), 3N, establish an interval where the eigenfrequencies can be excited. A suitable operating range for the wind turbine considered is chosen between 10-25 rpm. This definition of the operating range provides three different strategies, in order to avoid resonance issues, depending on the placement of the tower natural frequency. In case of fixing the eigenfrequency above the highest admissible frequency value, the tower is usually named as *stiff*. On the other hand, a *soft* design lies on placing the natural frequency of the tower in the N and 3N range. Lowering the first natural frequency below the entire operational range (minimum admissible frequency) results in the so-called *soft-soft* tower.

Both the soft and soft-soft schemes are advantageous economy wise (lower natural frequency means lighter designs, without external stiffening systems). This approach is widely accepted when designing tower made out of traditional material (such as steel and concrete). However, the inherent properties of wood demand a higher control over the material. Any source of vibration might lead to failure of the material due to the brittle nature of wood. Therefore, it might be problematic the brief period of time the tower is excited during the turbine start-up until the blades reach the rated output speed. Furthermore, particularly in this

situation, there is a tight margin where the natural frequency can be placed (for instance simply varying the mass of the structure affects the value of its natural frequency, having the designer a certain leverage over its final value), ranging between 0.51-0.42 Hz and 0-0.17 Hz respectively for the soft and soft-soft tower. Therefore, a conservative strategy is considered preferable for safety purposes even though, economy wise, it results less attractive. In order to design a stiff tower, the first mode frequency need to be moved away from the maximum operating frequency, which acquires a value equal to 1.25 Hz. A conventional security factor of 1.5 is considered, thus the real target equals 1.875 Hz.

In order to clarify the whole explanation, Figure 5.6 presents a Campbell diagram which showcases both the operating range and the different feasible strategies. A Campbell diagram is frequently used in turbine design to calculate values of eigenfrequencies as a function of the blades rotational speed. The black dashed lines represent the relation between frequency and rotational speed for both the 1N and 3N speeds (1N (rpm) =60*f (Hz) and 3N (rpm) =20*f (Hz)). The colored areas represent the different tower designs (stiff, soft or soft-soft). Finally, the horizontal blue line define the minimum allowable value for a stiff design (the one which this study aims to achieve), the yellow line marks the lower limit of the operating range and the green line represents the current natural frequency of the tower as it was mentioned in Section 5.2.

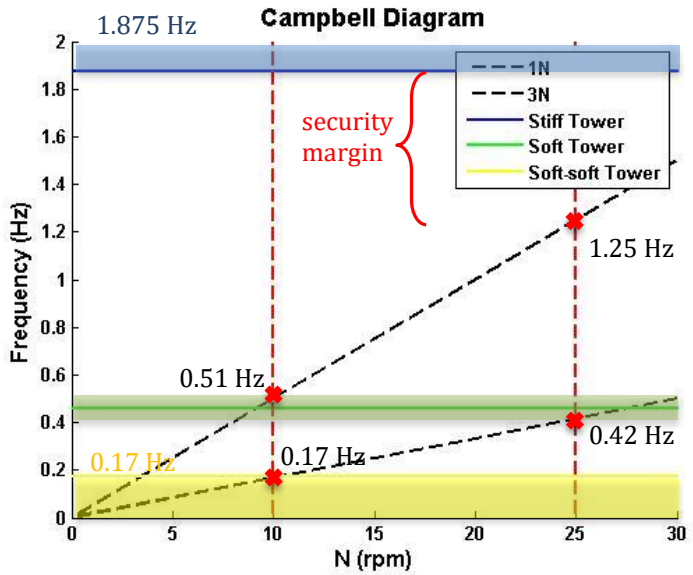

Figure 5.6 Stiff, soft and soft-soft strategies and operating range (dashed red lines), defined in a Campbell diagram.

In order to increase the natural frequency up to 1.875 Hz, the tower must be stiffen up by the inclusion of an external system. Two different alternatives are explained in-depth in the following sections. The first system is based on the attachment of crosswise wires between platforms, while the second opts for the construction of an internal space truss structure.

5.3.1 Wire-based system

A relatively simple and widespread way to increase the stiffness of a certain material is the introduction of cables either crossing through the material or being attached to the structure as external stiffeners. For this case study, the wires are anchored between consecutives platforms in a crosswise pattern. Due to space requirement for maintenance duties, only four cables, diametrically opposed, can be placed between two consecutives platforms. A sketch of the system is shown in Figure 5.7.

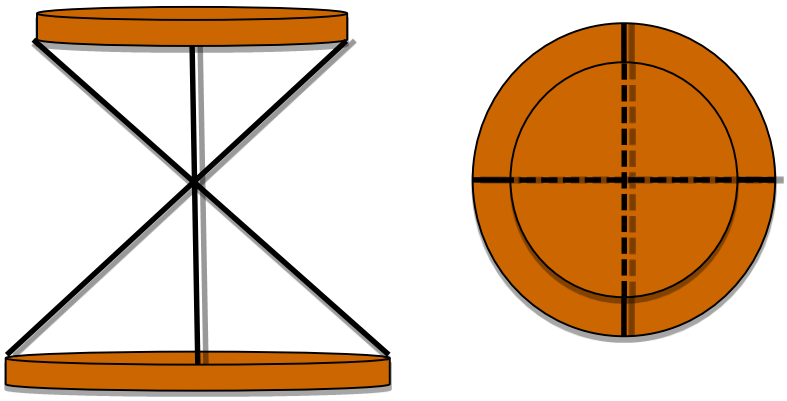

Figure 5.7 Layout of the crosswise cables between two platforms

An important factor which must be addressed when using cables is the lateral vibration of the wires as well as the consideration of the axial load derived from the pretension of the cables. The axial load directly affects the turbine and its reduction should be prioritized in order to decrease the cost of the whole structure. This vertical force must be withstood by the tower itself as well as foundation and bearings, hence the lower its value the better for the whole structure. However, reducing the axial load impacts the stiffness of the wires, therefore the required stiffness will restrict the decision making process.

It is clear that the design of wires is an iterative procedure which must take into consideration the behavior or response of the turbine, tower and further equipment. The following sections present a feasible design of the cables, in terms of strength, stiffness and lateral frequency without considering possible side effects due to the imposed tension on them (for instance, definition of the anchoring system to avoid failure of the wooden material due to transverse load). Nevertheless, such non-desirable effects can be easily solved, thus the investigation focuses on increasing the natural frequency of the tower in order to avoid resonance.

5.3.1.1 Cable parameters

Several parameters must be defined in order to design the wires. These parameters are the cross-sectional area, the number of cables, length of each cable, pretension, angle and the material (density and Young's modulus). For this matter, Table 5.4 presents the values for the selected cables. A definition of these

parameters is crucial in order to achieve the required strength and stiffness of the wire-based system as well as the desired increase in the tower stiffness.

Table 5.4 Number of wires per platform and mechanical properties of the material.

Number of cables/platform	4
Material	Carbon Fiber-Reinforced Polymer M55 UD
Density (kg/m^3)	1800
Tensile strength (MPa)	1600
Young's Modulus (GPa)	300
Diameter (m)	0.05

The inclination angle of the wires affects the length and, in turn, the stiffness of such elements. Due to the tapered design of the tower the inclination of the cables progressively increases with height becoming more parallel with the tower. Table 5.5 presents values of the angles, lengths and stiffnesses in regards to height.

Table 5.5 Angle, length and stiffness of each cable.

Level	**1**	**2**	**3**	**4**	**5**	**6**	**7**
Angle	46.34	49.22	52.36	55.79	59.54	63.59	67.95
Length(m)	20.73	19.81	18.94	18.14	17.40	16.75	16.18
Stiffness (MN/m)	28.41	29.73	31.10	32.48	33.85	35.17	36.40

The numbering on top of the table represents the platform levels in the tower. The highest level (between 105-120 m) remains free of cables in order to leave enough room for maintenance, placement of absorber devices, etc. Equations (5.1)-(5.3) present the procedure followed to calculate the values shown in Table 5.5.

$$\alpha_{\text{wire}} = \text{atan}\left(\frac{m}{r_{\text{o}}+r_{\text{next}}}\right) \quad (5.1)$$

$$L_{\text{wire}} = \frac{m}{\sin(\alpha_{\text{wire}})} \quad (5.2)$$

$$K_{\text{wire}} = \frac{E_{\text{wire}}\, S}{L_{\text{wire}}} \quad (5.3)$$

Where

α_{wire} Inclination angle of each cable [°]
L_{wire} Length of each cable [m]
K_{wire} Stiffness of each cable [MN/m]
E_{wire} Young's modulus [GPa]

S Cross-sectional area of a cable [m^2]
m Height between platforms. Constant value equal to 15 m
r_{o} Radius of the base platform in a certain level [m]
r_{next} Radius of the top platform in a certain level [m]

5.3.1.2 Carbon Fiber-Reinforced Polymer (CFRP)

A brief explanation of the reasons behind the selection of CFRP as the wires material along with several advantages and drawbacks upon traditional material is detailed throughout this section. The listed reasons are mostly based on the research presented by Armstrong Keith B., Bevan L. Graham, Cole William F. (2005).
One of the main goals of designing a timber tower lies in the significant reduction in weight in comparison with other materials, such as steel and/or concrete. Therefore, the need to select an alternative material as light as possible while fulfilling the strength and stiffness requirements is in line with this goal.
In structural engineering CFRP is used in several applications, such as strengthening concrete, timber structures or pre-stressing materials. Several advantageous reasons of the implementation of carbon fiber cables as a substitutive to traditional materials are presented in the following items:

- Reduction in weight due to a substantially lower density.
- Non-corrosive material, due to the non-metallic nature, resistance to chemical attack and outdoor weathering.
- Excellent strength-to-weight and stiffness-to-weight ratios.
- Superior properties compared to other fiber reinforced polymers (such as glass and aramid fiber-reinforced polymers).
- Long-term durability and fatigue resistance.
- Overall reduction in production and operational costs. Lower weight means lighter parts (such as the anchoring) which, in turn, results in economy savings.

However, it is necessary to mention some of the disadvantages with CFRP which, at some extent, overshadow the excellent characteristics of this material:

- High material cost.
- Transverse mechanical properties are substantially low in fiber composites (Baral N., Guezenoc H., Davies P., Baley C. [2008]).
- Complexity when being repaired or removed, due to possible damage of the fibers. It requires specific tools which increases the overall cost.
- In order to avoid the absorption of moisture by the matrices and fibers, the composite must be completely dried out.
- A thoroughly anti-contamination process must be carried out before each repair.

5.3.1.3 Simulation of the tower behavior adding the CRFP cables

A tower design with CRFP cables has been carried out in order to compute the new displacement, failure index and natural frequency of the tower. The wires were simulated by adding a spring connector with the specific spring constant and angle as shown in Table 5.5. Figure 5.8-Figure 5.11 display the new values for the

structure. As expected, the cables bring down both the maximum displacement and stresses in the tower, slightly increasing its first natural frequency.

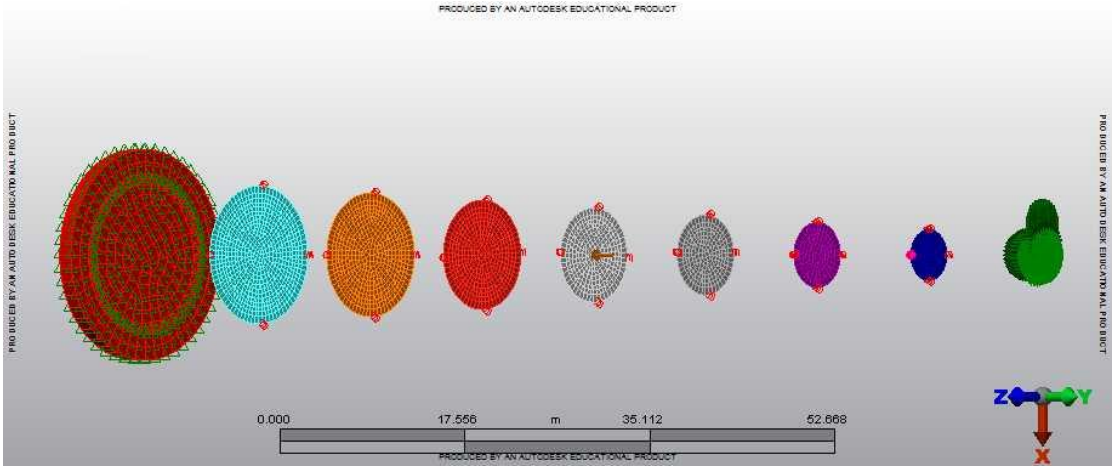

Figure 5.8 Spring connectors defined for each level of the tower with the software.

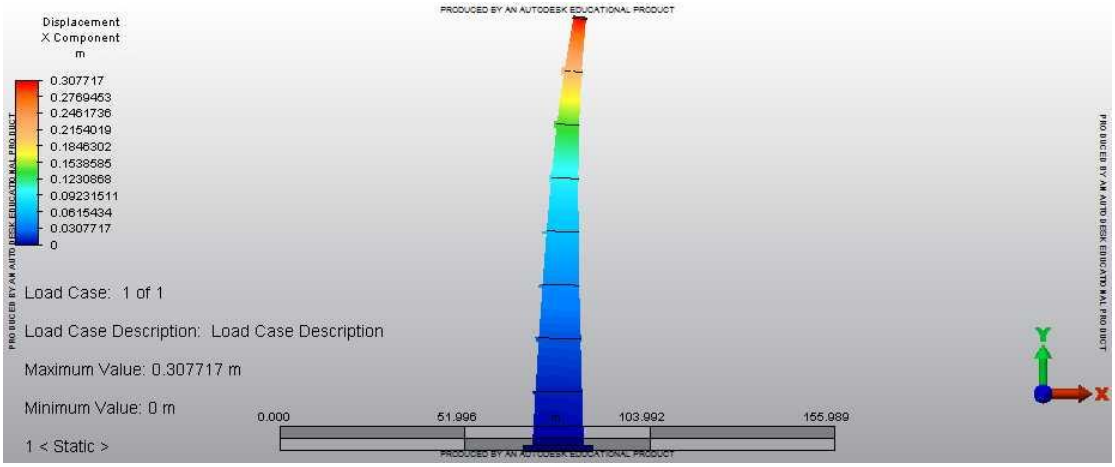

Figure 5.9 Top deflection of the 120 m adding CFRP cables.

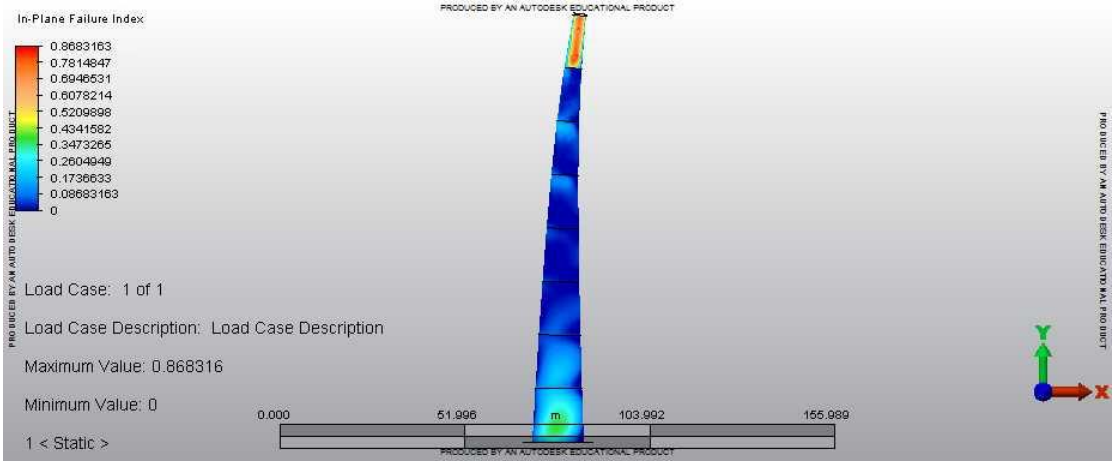

Figure 5.10 Failure index of the 120 m tower adding CFRP cables.

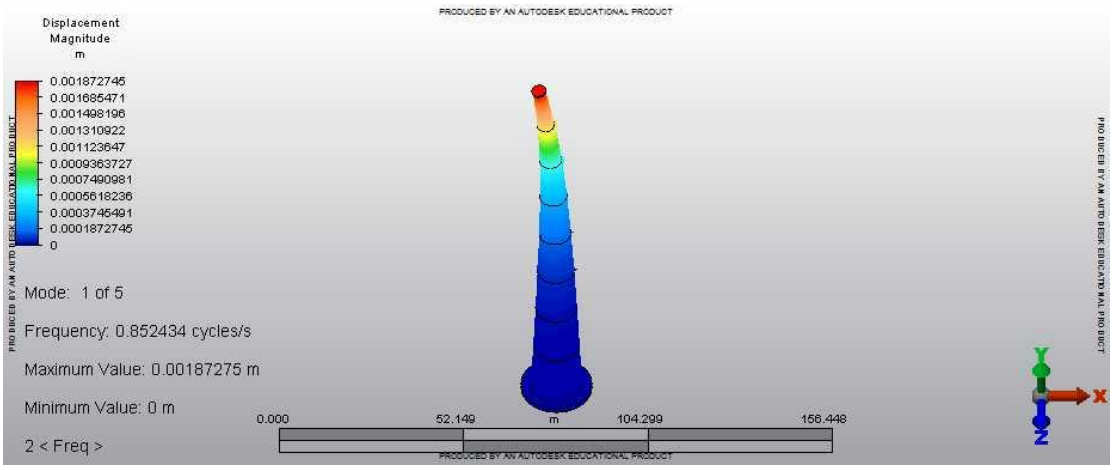

Figure 5.11 *1st natural frequency of the 120 m tower adding CFRP cables.*

Table 5.6 *Behaviour of the 120 m self-supporting tower vs the tower with CFRP cables.*

	Natural Frequency (Hz)	Failure Index	Deflection (m)
Self-supporting tower	0.55	2.09	1.15
Tower +CFRP cables	0.85	0.87	0.31

It should be noted that the proposed system solves the problem related with the failure index but it misses the mark in frequency terms. Since adding more cables would interfere with the space requirement, enlarging the cross-sectional area of each cable stands out as the main alternative to further stiffen up the tower. Figure 5.12 shows the tendency of the first natural frequency when increasing the diameter of the cable. The graph illustrates a linear relation between frequency and diameter. However, the low inclination of the curve imposes the use of extremely high cable diameter in order to match the frequency requirement for a stiff tower (1.875 Hz), leading to an undesirable cost increase. Therefore, a complementary passive damping system will be suggested in subsequent sections to solve the issue with the natural frequency.

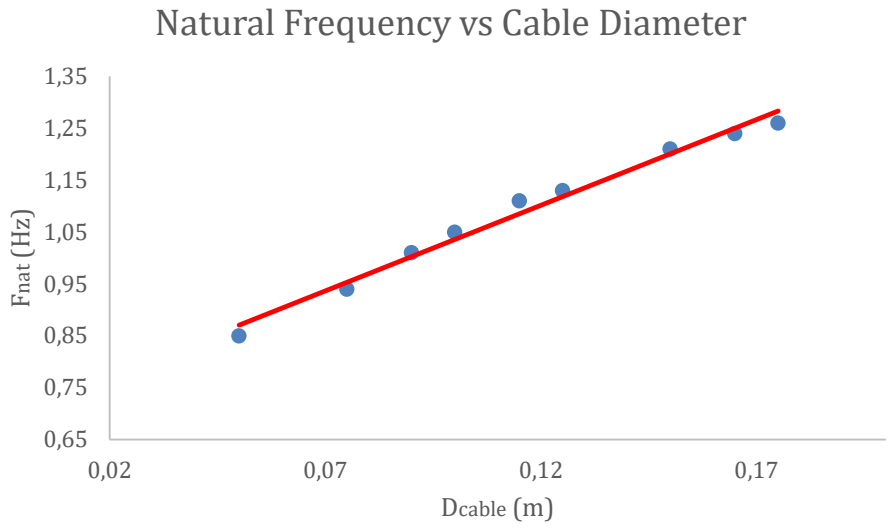

Figure 5.12 First mode frequency tendency with cable diameter.

5.3.1.4 Cable vibration and tensile strength

Lateral motion of the cables is a significant factor that needs to be considered in detail since it may potentially cause a catastrophic failure in the whole structure or a certain part of the tower. The natural frequencies of the cables can be calculated by modelling each element as a vibrating string. Equation (5.4) shows the general expression for any mode, in accordance to Carne T.G. (1980), even though this study is focused in the first natural frequency. If the first cable frequency is below 1.875 Hz then lateral vibration may occurred.

$$f_{\text{wire}} = n\frac{1}{2\pi}\sqrt{\frac{T}{\rho_{\text{wire}}S}} \tag{5.4}$$

Where:

n Mode number [-]
T Cable tension [N]
ρ_{wire} Mass density of the carbon fiber [kg/m^3]
S Cross-sectional area of the cable [m^2]

In order to fulfil the strength requirement, the cross-section of the cable must be large enough to withstand the turbine under strong wind situations (such as parked survival in hurricane winds). To ensure that the tension in the material does not exceed the ultimate strength a factor of safety must be selected. In accordance to Carne T.G. (1980), when the life span of the structure is expected to be over thirty years, it should be considered a minimum value of three for the factor of safety. Nevertheless, certain harmful and corrosive environments might force the consideration of a more conservative factor of safety in order to ensure a reliable functionality of the cables. Although the cables are not exposed to a hazardous atmosphere due to the protection given by the tower itself, the life span expected from them can easily be higher than thirty year, hence a conservative approach is preferable and the factor of safety is increased up to **4**. There is not a

precise value for the factor of safety, it is up to the designer to choose the most suitable one according to the case study.

The main issue is that the tension in the cables varies with the wind load and temperature, hence it becomes a challenging task to completely avoid resonance in any case. Cable tension can be broken down into two different components (as shown in equation 5.5): T_p which is the pretension and T_w which is the increase caused by the wind load (or any external action), forcing the tower to bend. The latter can be estimated as given by equation 5.6 (Möllerström E., [2015]).

$$T = T_p + T_w \tag{5.5}$$

$$T_w = K_{wire} \Delta Z cos\alpha_{wire} \tag{5.6}$$

Where:
ΔZ Horizontal deviaton undergone by the wire [m]

In order to ensure a reliable serviceability of the cables an approximate estimation of the maximum tension that they can withstand is performed by defining the maximum horizontal deviation (on top of the tower) and then, comparing the result obtained in equation 5.5 with the value given by equation 5.7.

$$T_{adm} = \frac{R_m S}{F_{saf}} \tag{5.7}$$

where:
T_{adm} Maximum admissible tension in the wire [N]
R_m Tensile strength of the material [Pa] (see Table 5.4)
F_{saf} Factor of safety [-]

Figure 5.13 illustrates the values of both the admissible tension and the actual tension in the cable as a function of cable diameter. In order to calculate the tension in the wires, the deflection undergone by the cables in the highest level of the tower has been chosen as the reference value. Furthermore, a value of 100 kN has been fixed as the pretension for the cables. Several simulations, varying the cross-sectional area, has been carried out to plot the graph.

Plots clearly show a minimum diameter from which the tensile strength divided by the factor of safety is not surpassed. This value lies around 0.09 m, which might be slightly larger than the optimal size. Nevertheless, considering a time span lower than thirty years and a well-protected system, a less conservative value for the factor of safety can be selected. Such measurement would substantially decrease the diameter where both curves cross (approximately down to 0.06 m).

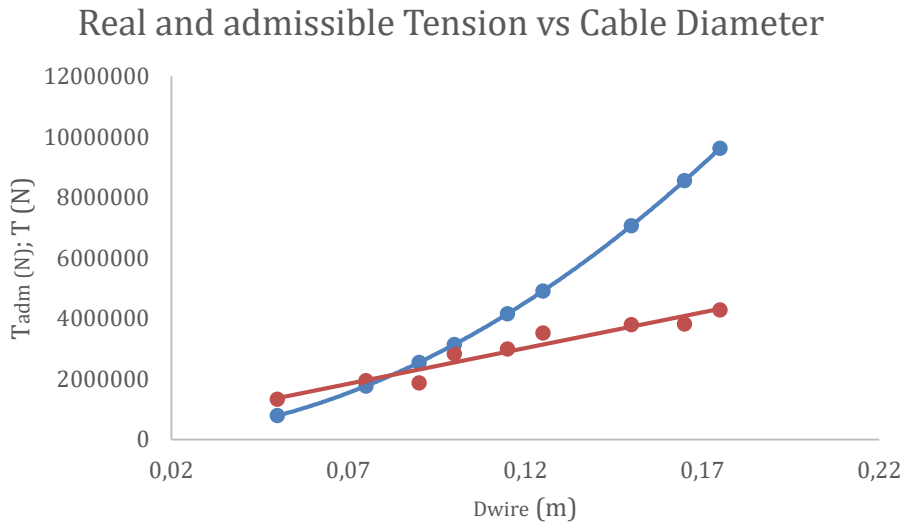

Figure 5.13 *Admissible (blue solid line) and real cable tension (red solid line) as a function of cross-sectional area.*

The next step involves the study of the first natural frequency. Resonance is avoided if this value is placed above the primary excitation frequency (1.25 Hz, see Figure 5.6). However, such strategy may be economically unviable, especially for large turbines. It will be presented the range of frequencies where resonance might occur, for two different configurations as shown in Table 5.7. It is important to remark that the maximum deflection is undergone by cables in line with wind (both windward and leeward), thus the upper and lower limits of the aforementioned frequency range are limited by them (the excitation frequency of any wire, independently to its angle towards wind, is covered inside such interval, Möllerström E., [2015]). A negative deflection, $-\Delta Z$, allows the estimation of the natural frequency of leeward cables.

Table 5.7 *Natural frequency for a windward and leeward cable at different tower levels with two different diameters: 0.09 and 0.175 m.*

Level/Diameter	**D_{wire}=0.09 m**		**D_{wire}=0.175 m**	
	Windward	**Leeward**	**Windward**	**Leeward**
1	11.6	0 +11.1i	9.1	0+8.9i
2	12.1	0 +11.5i	9.4	0+9.3i
3	12.5	0 +12.0i	9.8	0+9.6i
4	12.7	0 +12.3i	10.0	0+9.8i
5	12.9	0 +12.4i	10.1	0+9.9i
6	12.8	0 +12.3i	10.0	0+9.8i

7	12.5	0 +11.8i	9.7	0+9.5i

The complex numbers referred to the leeward cable means that this element goes slack due to the large horizontal deviation. However, it does not mean that the wire cannot be excited. In fact, the interval where resonance might occur ranges from 0 Hz to 12.9 Hz (or 10.1 in the other case).

The frequency issue cannot be solved by increasing the cross-sectional area of the wire as shown in Table 5.7. Hence, two approaches can be followed to resolve this issue: either increase the pretension in the wires or introduce a simple damping system for each cable (see section 5.3.1.5). The main consequence of a higher pretension is the stress caused in the anchoring system as well as the material where the system is attached. Furthermore, as mentioned in Section 5.3.1, the axial load imposed by the cables leads to a more stressed structure. Therefore, a straightforward and simple damping system is proposed in the subsequent section to mitigate the vibration problem.

5.3.1.5 Damping system for cables

Since vibrations of cables always exist and due to the low inherent damping coefficient of these elements (less than 0.2 % of critical), an external damping system is considered. The proposed damping system has been designed and tested by Carne T.G. (1980). The basic principles of this concept are summarized in the following items:

- The method to dissipate energy is based on Coulomb friction model.
- It is constituted by a pair of weights lying over two inclined surfaces and sliding with the cable movement.
- Simple, reliable and cost effective system. Furthermore, it demands little maintenance.
- The resulting damping coefficient is estimated by analysing the physical system (as shown in Figure 5.14).
- Only the in-plane motion is considered. Out-of-plane motion is uncoupled (small level of vibration is assumed) .
- The suitable magnitude for the weights is obtained by equating the energy dissipated with viscous damping and Coulomb friction (due to the assumption of viscous damping when calculating the aforementioned damping coefficient). Figure 5.14 illustrates a simple system for both cases.

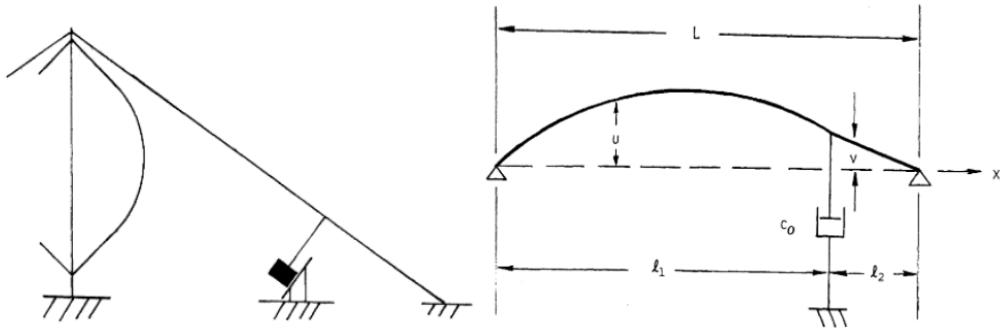

Figure 5.14 *a) Diagram of cable damping concept; b) Diagram of cable with damper. Reproduced from: Guy Cable Design and Damping for Vertical Axis Wind Turbines: Sandia National Laboratories, energy report.*

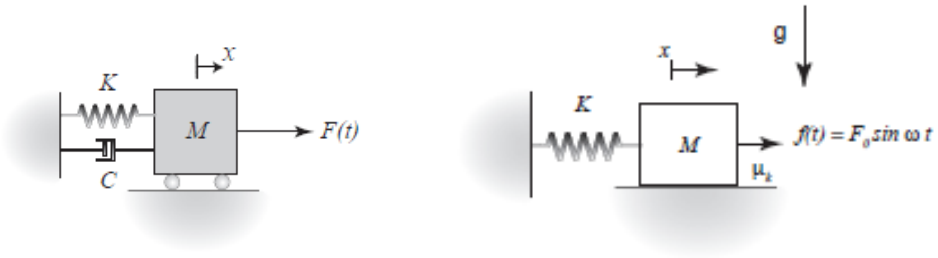

Figure 5.15 *a) Forced mass-spring-damper system; b) Simple Coulomb friction model. Reproduced from: Dr. S. Stutts, Daniel: Equivalent Viscous Damping.*

These principles lead to the definition of two expressions (as stated by Carne T.G. (1980)), as shown in equations (5.8) and (5.9), which allows to the calculation of the desired damping coefficient and required weights.

$$\zeta = \frac{\pi c \lambda^2}{1+\pi^2 c^2 \lambda^2} \tag{5.8}$$

$$W = \frac{c_0 \pi \omega u(x_0)}{4\mu cos\gamma} \tag{5.9}$$

where:

ζ Damping coefficient achieved with the weights [-]

W Mass of the weights placed on the surfaces [kg]
ω Natural frequency of vibration of the cable [rad/s]
μ Friction coefficient [-]
γ Elevation angle of the friction surface [°]
$u(x_0)$ Displacement of the cable at the attachment [m]
c Factor given by equation 5.10:

$$c = \frac{c_0}{\sqrt{T \mu_{wire}}} \tag{5.10}$$

where:

c_0 Viscous damping coefficient [-]
T Tension of the cable [N]

μ_{wire} Mass per unit length [kg/m]
λ Factor given by equation 5.11 [-]:

$$\lambda = \frac{l_2}{L_{\text{wire}}} \tag{5.11}$$

where:
l_2 Distance between one end and the damping system as shown in Figure 5.14 [m]

Special attention should be paid when analysing the sliding weight because of the nonlinearity of friction damping (c_o decreases with increasing amplitude, $u(x_o)$. Therefore, it is important to anticipate a value for such displacement). Equation 5.8 is represented in Figure 5.16, showing a series of curves of the damping coefficient as a function of c, for different values of λ. By simply placing the weight one-tenth of the distance along the cable ($\lambda = 0.1$), a damping coefficient up to 5% can be achieved (25 times higher than the inherent damping of the cable). For the study case, the damping system could even be connected in the middle of the element (where the wires cross each other), obtaining a substantial increase in the damping coefficient (up to 25% as it can be derived from Figure 5.16).

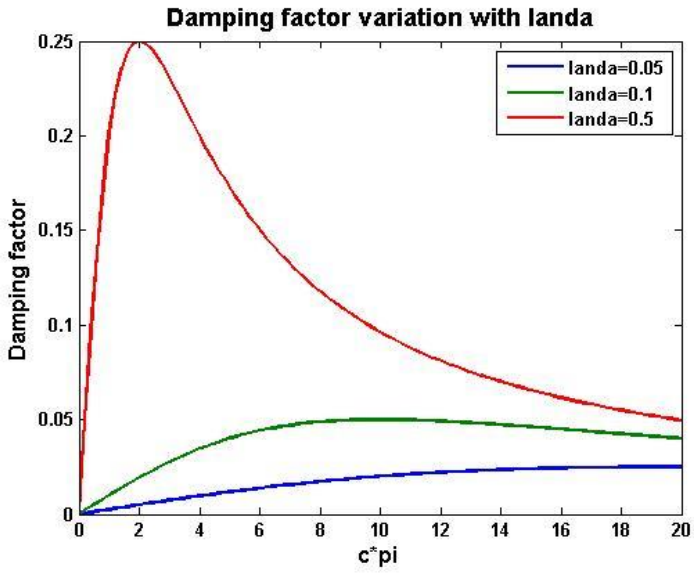

Figure 5.16 Variation in damping factor with viscous damping coefficient. Modified from the original: Guy Cable Design and Damping for Vertical Axis Wind Turbines: Sandia National Laboratories, energy report.

In order to define the mass of the weigths with accuracy testing in the cable should be carried out and an estimation of the maximum expected displacement must be obtained. Nevertheless, the small value of such weights (between 5 and 10 kg) would not affect the behavior of the tower at all.

5.3.1.6 Tuned vibration absorber (TVA)

A way to ensure a reliable operability throughout the tower lifetime, when using the wire-based system, depends on avoiding resonance of the structure with the loads of the passing blades. Since the cables are not able to increase the first

natural frequency up to the targeted value of 1.875 Hz, an additional damping system must be placed on top of the tower.

Tuned vibration absorber (TVA), which basic principle consists on a moving mass and a spring with a certain damping coefficient, is a successful invention for vibration mitigation. It is widely used in civil and structural engineering (bridges, tall buildings, pipelines, etc.) as well as different kind of industrial machinery and other mechanical systems.

TVAs tend to lose effectiveness with time, due to the variable nature of the operating conditions of the considered device/structure, reason for what more advanced systems has been developed. It can be distinguished four different categories of TVAs: passive, adaptive, semi-active and active systems.

Due to the wide variety of devices available nowadays and the complexity to design a system which maintains constraints of weight, size and cost, in general, it is not a matter for this study to present an extensive survey and/or propose a working model. Martynowicz P. [2015] proposed a TVA model for vibration control of a wind turbine tower-nacelle based on magnetorheological tuned vibration absorber (MHTVA). A MHTVA is a semi-active device able to adapt its properties as the operating conditions of the low-damped tower fluctuate with time. To illustrate the diversity of these devices, an interesting example is the installation of a tuned liquid column damper, consisting of a U-shaped tank filled with a Newtonian liquid, as Altay O., Butenweg C., Klinkel S. and Taddei F. proposed on their research ("*Vibration Mitigation of Wind Turbine Towers by Tuned Liquid Column Dampers*", [2014]).

5.3.2 Space truss

A second approach to fulfill the requirements regarding resonance consists of adding an inner space truss structure to the already defined outer CLT structure. Different solutions can be reached. The one proposed in this section can be seen in Figure 5.17.

A few aspects of the design deserve to be mentioned:

- The structure consists of 9 levels, 7 of them correspond to each one of the inner platforms. The remaining 2 correspond to both ends of the tower (foundation and top of the tower). That covers the 120 m height ((9-1) platforms * 15 m/platform = 120 m).
- Each level has been designed as a pentagonal shaped truss. A squared or hexagonal truss might work as well, however a pentagon adjusts to a circumference closer than a square (gives more room left in the inside) and doesn't require as many truss elements as a structure based on hexagons. With the pentagon-based space truss, the angle of diagonal truss elements with respect to the horizontal plane (X-Z plane) ranges from 62.5° (bottom level) to 81.7° (top level). Angles derived from an hexagon-based space truss would be higher, which is not desirable.

- Notice that, according to Modvion's patent, the tower should be a self-supporting structure. Hence the addition of an inner structure as a design solution is not considered optimal.

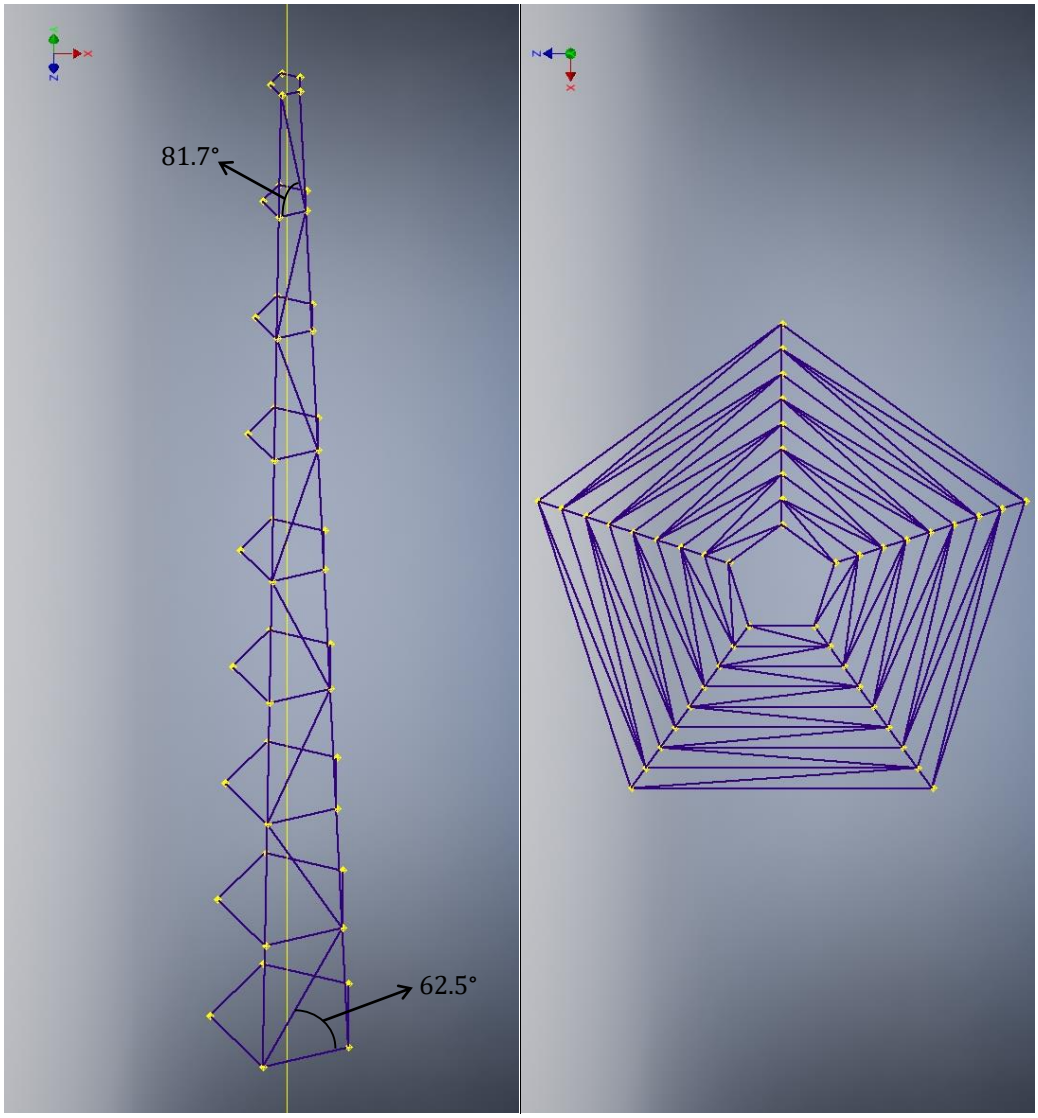

Figure 5.17 Proposed space truss inner structure for the 120 m tower.

The proposed inner structure has been implemented and is shown in Figure 5.18. Each one of the truss elements included in the framework corresponds to a 40 mm outer diameter tube with a 4 mm thickness wall.

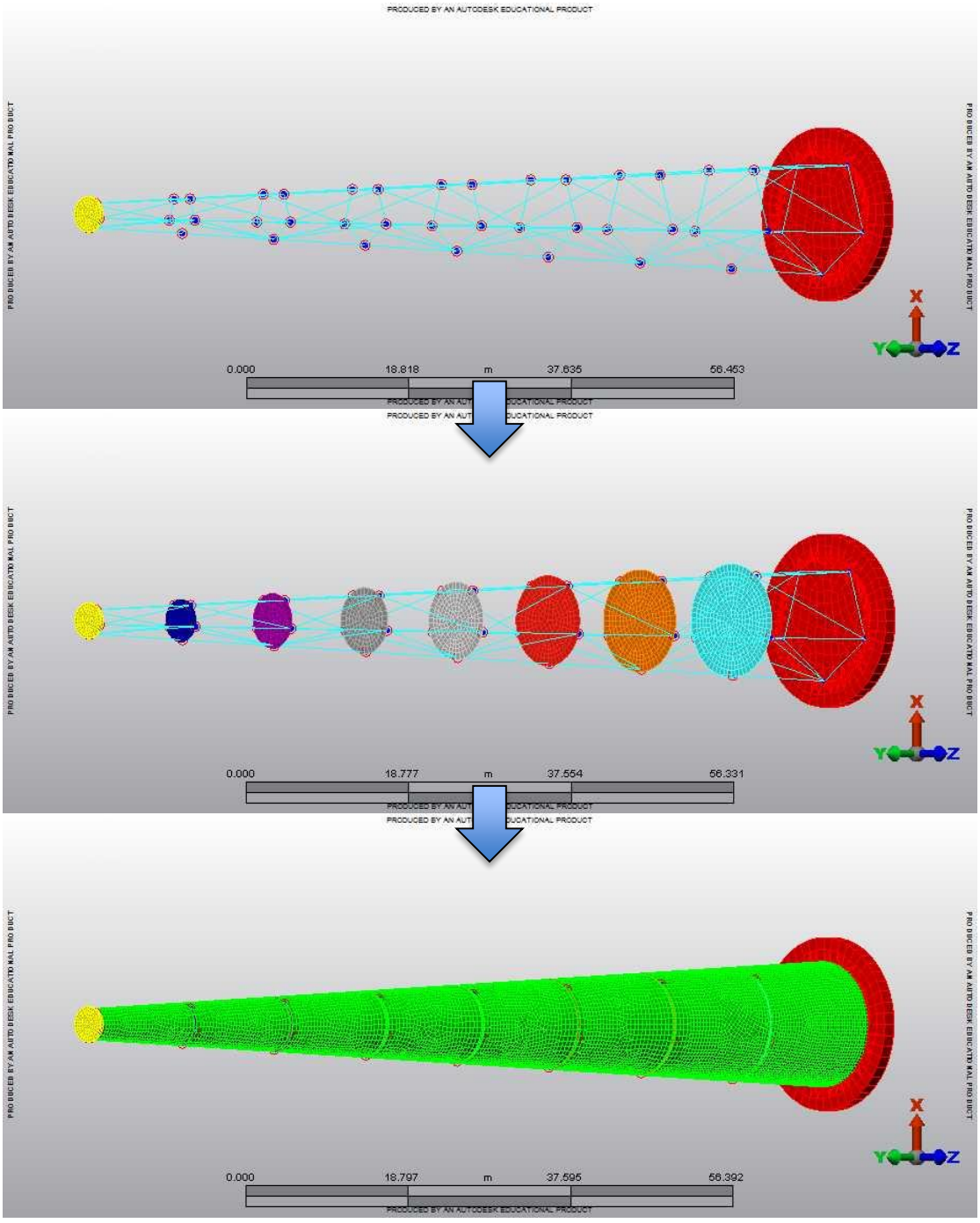

Figure 5.18 Implementation of the inner space truss structure in the FE model of the 120 m tower.

With the aid of the proposed space truss structure, frequency issues can be easily solved as shown in Figure 5.19.

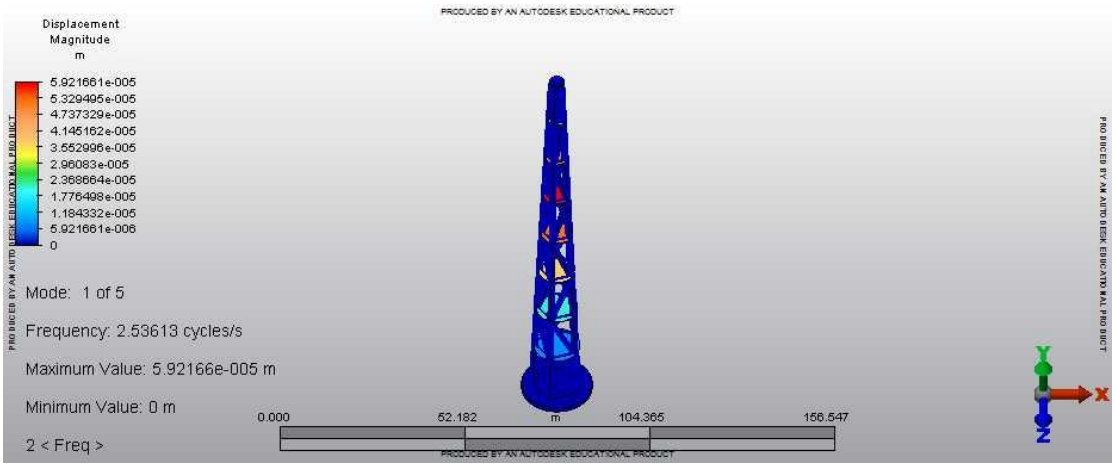

Figure 5.19 Frequency analysis of the 120 m tower equipped with the inner space truss structure showing the value of $f_{\text{nat},1}$.

By adding an inner structure design similar to the proposed one, it is easier to design a *stiff* tower according to what have been described in Section 5.3 ($f_{\text{nat},1}$ >1.875 Hz).

6 Proposed 3d model for the 120 m tower

Despite having considered the tower as a whole throughout the numerous studies carried out along this project, it is clear that the real design consists of several wooden modules that fit into each other as if it were a puzzle.

This section introduces the final CAD model of the assembly and explains how the modular structure is assembled.

The FE software automatically identifies contacts (or their absence) between parts thus checking whether the designed modules perfectly fit or not is possible. Notice the existence of difficulties when it comes to designing each module due to the existing curvature and the certain angle of inclination (α) derived from the truncated-cone shape of the tower plus the rabbet system employed for assembling them.

6.1 3D model of a generic module

A generic wood module, as it was introduced in Section 2.4, is shown in Figure 6.1:

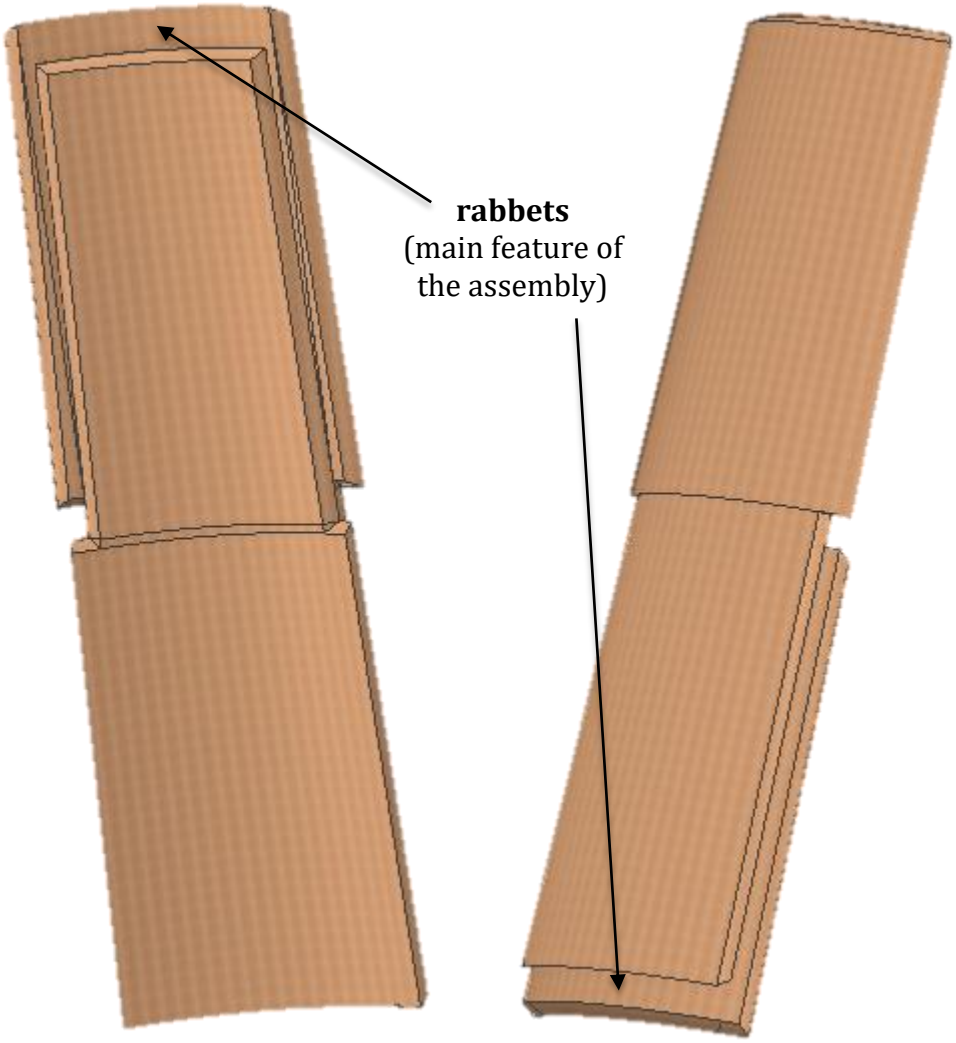

Figure 6.1 Aspect of a generic timber module.

A few aspects of the design of the module that should be addressed are:

- For transportation and handlig reasons, 6 modules will be installed per cross-section (see Figure 6.2).

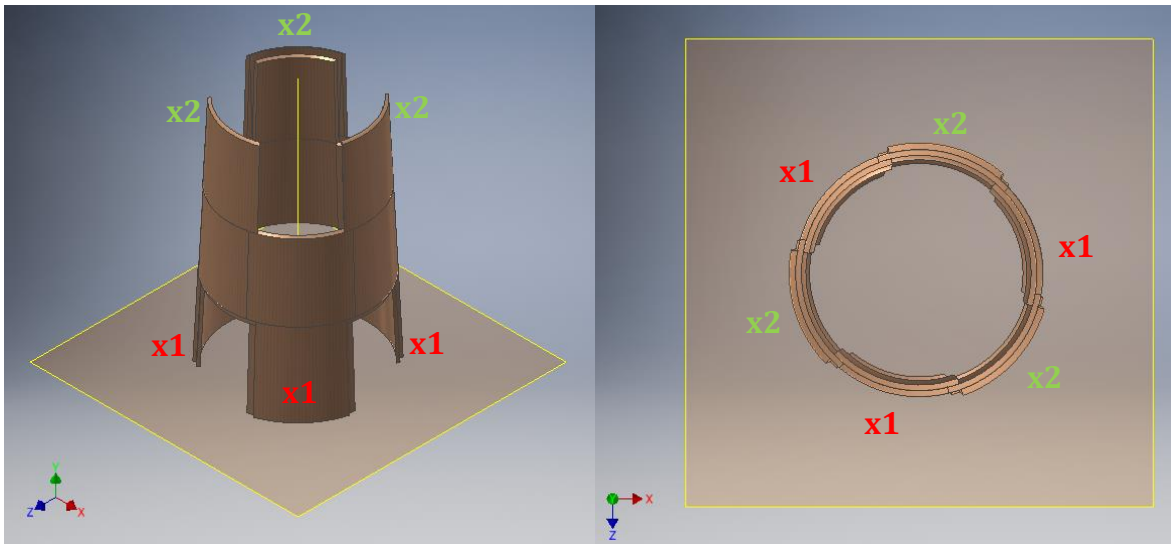

Figure 6.2 Cross-section of the assembly.

- The outer structure is formed by 51 wooden modules that perfectly fit into each other. There are 17 groups of modules (a0, a1, a2, b1, b2, c1, c2, d1, d2, e1, e2, f1, f2, g1, g2, h1 and h0). Each group is formed by 3 modules equal to each other in terms of geometry. Regarding the nomenclature, every cross-section belongs to a letter (see "x1" and "x2" in Figure 6.2). The zero in "a0" and "h0" makes reference to a group of trimmed modules (half of the height of a regular one i.e. 15 m / 2 = 7.5 m). Trimmed modules are necesary at the bottom and at the top of the tower to ensure flatness and a good fit at both ends of the structure. This layout can be easily understood by observing Figure 6.3:

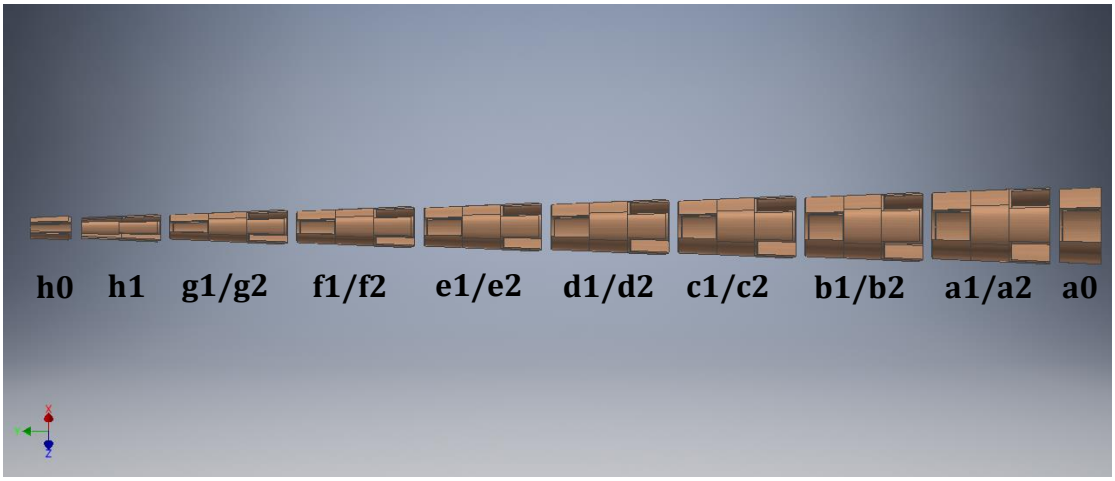

Figure 6.3 Assembly process of the 120 m tower built out of 51 modules.

- Every module has been designed as a parametric 3D geometry (see Figure 6.4), i.e. each module's dimensions can be easily altered to fit a tower with a different height, bottom/top diameter and so on.

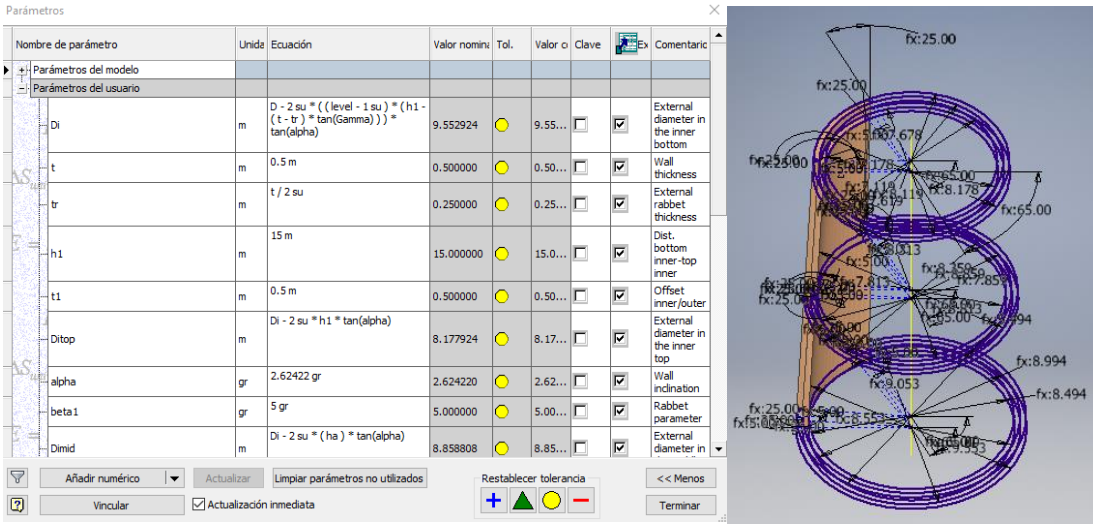

Figure 6.4 Some of the parameters associated to the parametric design of a module.

6.2 3D model of the assembly of the outer structure

Once the 51 modules have been successfully assembled, the resulting tower looks like it is shown in Figure 6.5:

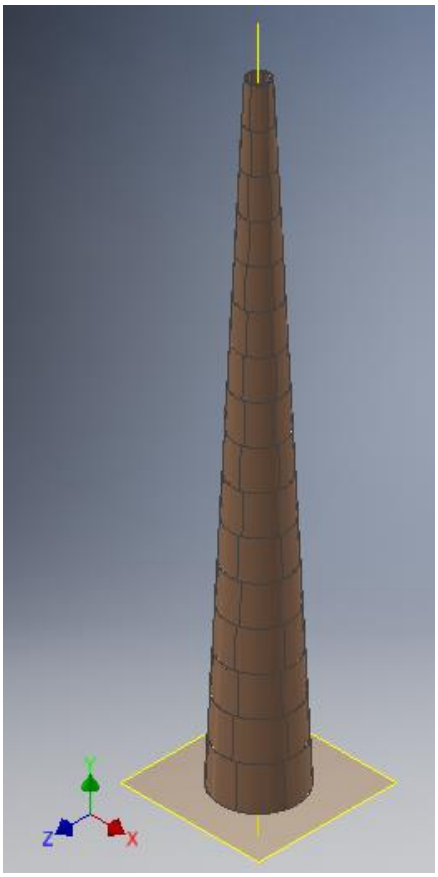

Figure 6.5 Assembly of the outer structure of tower built out of 51 CLT modules.

6.3 Considerations regarding the 3d model

Regarding the current patent-pending status of the technology developed by Modvion, no blueprints of the 17 module types are provided.

7 Discussion and conclusion

Some of the main challenges and outcomes encountered/obtained throughout the completion of the project have been:

- Designing 4 feasible self-supporting towers with a hub height below the 120 m target (Section 4.3).
- Proposing 2 alternative designs for a feasible 120 m tower based on different systems and support structures (Section 5.3).
- Geometrically comparing the rounded cross-section of the studied designs to the octagonal shape used by the competence (Section 4.4).
- Parametrically modelling the 3D geometries of each and every one of the 51 timber modules that, once assembled, constitute the self-supporting structure of the 120 m tower (Section 6).
- Fulfilling the initial given requirements.
- Fulfilling those requirements arisen after the start of the thesis work. Notice that the project hadn't been fully defined in the beginning, so meetings have been frequently held in order to update the idea according to new needs/ideas coming from Modvion or new requirements imposed by the manufacturers.

Regarding the design process of the tower, a few decisions could be discussed and considered for further optimization of the model in the future:

- Different strength classes of wood might be implemented into the composite in order to achieve a better performance, rather than sticking with the default materials given by the manufacturer. Similarly, the layup of the composite may be further optimized.
- There are additional failure theories that may be worth checking besides Tsai-Wu's in order to ensure the endurance of the composite.
- Wind has been studied as a static load according to what is dictated in the used standards. A more detailed analysis would include wind tunnel simulations addressing the dynamic nature of the wind load.
- Top loads coming from the turbine have been selected from a safety point of view from reference values. A more proper approach would include the selection of a commercial turbine and the calculations of the top loading state.
- Boundary conditions related to the ground should be further studied since, through this project, the foundation has been considered perfectly fixed to the ground. Even though conducting further research concerning this topic is not expected to have large effect on the final solution, it is advised to do so since its effects, although unlikely, might be critical.

Overall, most of the design choices have been taken in compliance with the restrictions and requirements imposed by the manufacturers and the company (Modvion). The final conceptual designs include several parameters that might – and should – be optimized having in mind aspects such as costs. What is eventually presented as *final designs* (see Section 0) are nothing but feasible solutions that would accomplish the ultimate goal of obtaining a 120 m tower design, as well as serve as a guide for subsequent researchers or designers.

As a conclusion, and as an answer to Modvion's concerns and initial question regarding the feasibility of building a 120 m wind turbine tower based on the patent pending technology, the authors state:

The 120 m tower is feasible, as long as the guidance provided in this document is followed. Note that, unlike the claims found on the patent, a self-supporting structure based on the CLT modules on their own wouldn't be as useful as expected as a wind turbine tower.

8 Annex I: Matlab scripts

8.1 Wind profile

```
%% EUROCODE 1 1991-4-1-1
%% INPUT DATA
Z0= 0.05; % Roughness of the terrain. It was taken from table 4.1
(Category II)
ro=1.21933; % Air density (kg/m^3). Taken from ISO 2533
h=120; % Initial hub height (m). Assumption to estimate Reynolds
number.
b= 12; % External base diameter (m)
btop=12/3; % External top diameter (m)
t=0.3; % thickness of the wall (m)
v= 15*10^(-6); % Kinematic viscosity of air (m^2/s)
ro_m=400; % Material density (kg/m^3)
syms Z; % Height (m)

%% VELOCITY AND PEAK PRESSURE
% a) Basic wind velocity
vb=25; % Basic wind velocity (m/s).

% b) Mind wind velocity
C0=1; % Orography factor. It is considered equal to the unity unless
other requirements should be fulfilled.
Zmin=2; % Minimum height above ground level.
ZI=0.05; % Roughness of the terrain for category II.
Kr=0.19*(Z0/ZI); % Terrain factor depending of the roughness of the
terrain.
Cr1=Kr*log(Z/Z0); % Roughness factor for Zmin=2m <= Z <= Zmax=200m.
Cr2=Kr*log(Zmin/Z0); % Roughness factor for Z < Zmin=2m.
vm1=Cr1*C0*vb; % Mean wind speed as a function of height (m/s)for
Zmin=2m <= Z <= Zmax=200m.
vm2=Cr2*C0*vb; % Mean wind speed as a function of height (m/s)for Z <
Zmin=2m.

% c) Wind turbulence
KI=1; % Turbulence factor. Recommended value.
Sigmav=Kr*vb*KI; % Wind deviation (m/s).
Iv1= KI/(C0*log(Z/Z0)); % Turbulence intensity as a function of height
for Zmin=2m <= Z <= Zmax=200m.
Iv2=KI/(C0*log(Zmin/Z0)); % Turbulence intensity for Z < Zmin=2m.

% d) Peak velocity pressure
qp1=(1+7*Iv1)*0.5*ro*vm1^2; % Peak velocity pressure (Pa) for Zmin=2m
<= Z <= Zmax=200m.
qp2=(1+7*Iv2)*0.5*ro*vm2^2; % Peak velocity pressure (Pa) for Z <
Zmin=2m.

%% CIRCULAR CROSS-SECTION
%% PRESSURE PROFILE
Ze=h;
Cre=Kr*log(Ze/Z0); % Roughness factor for the reference height.
Vre=Cre*C0*vb;
Re=b*Vre/v % Reynolds at the reference height Ze=h.

% a) Gamma factor
landa=0.7*h/b; % Slenderness factor
if landa<= 70
   landa=0.7*h/b;
```

```
else landa=70;
end
phi=1; % Solidity ratio
Gammaend=0.75;  % Figure 7.36. End-effect factor. Functions of
slenderness and solidity ratio (for cylindrical shapes).

% b) Coefficient of pressure
syms alpha
alpha_A=105*pi/180;
alpha_min=75*pi/180;
gamma_1=1;
gamma_2=Gammaend+(1-Gammaend)*cos(pi/2*(alpha-alpha_A/(alpha_A-
alpha_min)));
gamma_3=Gammaend;
Cpo1=1E-05*alpha^3-0.0016*alpha^2+0.007*alpha+1;
Cpo2=0.0008*alpha^2-0.128*alpha+3.4445;
Cpo3=-0.8;
Cp=2*int(gamma_1*Cpo1*cos(alpha),0,alpha_min)+2*int(gamma_2*Cpo2*cos(
alpha),alpha_min,alpha_A)+2*int(gamma_3*Cpo3*cos(alpha),alpha_A,pi);
% External coefficient of pressure obtained as the integration of the
pressure distribution over the cross-section of the cylinder.
Cp=double(Cp)

% c) Pressure
We1=qp1*Cp; % External pressure for Zmin <= Z <= Zmax.
We2=qp2*Cp % External pressure for Z < Zmin.
We1=simplify(We1)
Znum1=linspace(2,200,100);
Znum2=linspace(0,2,20);
We1_num=subs(We1, Z, Znum1);
We2_num=subs(We2, Z, Znum2);
hold on;
plot(We1_num, Znum1, We2_num, Znum2, 'linewidth', 2,'linewidth', 2)
set(gca,'fontweight','bold')
xlabel('Pressure (Pa)','fontsize',12)
ylabel('Height (m)','fontsize',12)
title('Wind Profile','fontsize',14)
hold off;
```

8.2 Wire-based system

```
clear all;
close all;
clc;

%% Campbell Diagram
N=0:10:30;
f1=N./60;
f3=N./20;
figure
co = get(gca,'ColorOrder') % Initial
% Change to new colors.
set(gca,'fontweight','bold', 'ColorOrder', [0 0 0; 0 0 0; 0 0 1; 0 1
0; 1 1 0; 1 0 0; 1 0 0], 'NextPlot', 'replacechildren');
co = get(gca,'ColorOrder') % Verify it changed
plot(N,f1,'--',N,f3,'--
',[0,30],[1.875,1.875],[0,30],[0.46,0.46],[0,30],[0.17,0.17],[10,10],
[0,2],'--',[25,25],[0,2],'--','linewidth',2)
title('Campbell Diagram','fontsize',14);
xlabel('N (rpm)','fontsize',12);
ylabel('Frequency (Hz)','fontsize',12);
```

```
legend ('1N','3N','Stiff Tower','Soft Tower','Soft-soft Tower')

%% INPUT DATA
Ew=300000000000; % Young's Modulus wires (Pa)
ro_w=1800; % Density of carbon fiber (kg/m^3)
dw=0.05; % Wire diameter (m)
alpha=180-(90+2.62); % Tower inclination
H=120; % Tower height (m)
m=15; % Module height (m)
h=H-m; % Maximum height where wires are fixed (m)
n=round(H/m-1); % Effective number of wires in a certain direction
t=0.5; % Tower width (m)
Db=15; % Bottom diameter of the tower (m)

%% Effective and real stiffness
A=pi*dw^2/4; % Wire cross-sectional area (m^2)
rnext=Db/2; % Initial reference radius (m)
mtot_w=0;
f=1;
for i=1:n
    r1=rnext;
    rnext=Db/2-i*m/tan(alpha*pi/180);
    alpha_wire_i=atan(m/(r1+rnext)); % Angle of each cable over the
horizontal axis
    Lw_i=m/sin(alpha_wire_i); % Wire length (m)
    kwire_i=Ew*A/Lw_i; % Stiffness of each wire (N/m)
    m_wire=4*n*A*Lw_i*ro_w; % Mass of each wire (kg).
    mtot_w=mtot_w +m_wire; % Total mass of the wires (kg)
    Lw(f)=Lw_i;
    kwire(f)=kwire_i;
    alpha_wire(f)=alpha_wire_i;
    f=f+1;
end

%% Natural frequency of the wires
Rm=1600; % Tensile strength of M55 UD carbon fiber (Mpa)
FS=4; % Safety factor
Tpad=Rm*10^6*A/FS; % Maximum admissible tension in the wire (N)
Tp=100000; % Pre-tension of the wire (N)
mu=ro_w*A; % Linear density (kg/m)
deltaZ=0.26; % Maximum admissible horizontal displacement (m. It
varies depending on the wire diameter. For d=0.05 m, it is equal to
0.26
fnat_wire_windward=1./(2.*Lw).*sqrt((Tp+kwire.*deltaZ.*cos(alpha_wire
)).*/mu)
fnat_wire_leeward=1./(2.*Lw).*sqrt((Tp-
kwire.*deltaZ.*cos(alpha_wire)).*/mu)

%% Damping system
syms landa c
damp=(pi*c*landa^2)/(1+pi^2*c^2*landa^2);
Ddamp=diff(damp,c);
Values=(solve(Ddamp==0,c)); % Value of c at which the damping factor
is at its maximum for any feasible value of landa.
cpi_num=linspace(0,20,100);
damp_num=(cpi_num.*landa^2)./(1+cpi_num.^2.*landa^2);
Damp_landa1=subs(damp_num,landa,0.05);
Damp_landa2=subs(damp_num,landa,0.1);
Damp_landa3=subs(damp_num,landa,0.5);
figure
```

```
plot(cpi_num,Damp_landa1,cpi_num,Damp_landa2,cpi_num,Damp_landa3,'lin
ewidth', 2)
set(gca,'fontweight','bold')
title('Damping factor variation with landa','fontsize',14);
xlabel('c*pi','fontsize',12);
ylabel('Damping factor','fontsize',12);
legend ('landa=0.05','landa=0.1','landa=0.5')
```

9 References

- Porteous J., Kermani A. (2007): *Structural timber design to Eurocode 5.* Blackwell Publishing Ltd, Oxford, UK, 2007, pp. 1-15 and 119-120.
- Gagnon S., Pirvu C. (2011): *CLT Handbook,* FPInnovations, Québec, Canada, 2011, Chapters 1 and 3.
- Roylance D. (2000): *Laminated composite plates*. Department of Material Science, Massachusetts Institute of Technology, Cambridge, USA, 2000, pp. 1-3.
- Mohammad M., Gagnon S., K. Douglas B., Podesto L. (2012): *Introduction to Cross Laminated Timber*. Wood Design Focus, Vol. 22, No. 2, summer 2012.
- S. Taranath, B. (2012): *Structural Analysis and Design of Tall Buildings: Steel and Composite Construction*. CRC Press, Boca Raton, Florida, USA, 2012, pp. 215-218.
- D. Blevins, R. (2001): *Formulas for natural frequency and modeshape.* Krieger Publishing Company, 2001 (Reprint Edition).
- Eurocode 1 (2005): *Action on Structures, General actions, Part 1-4: Wind actions*, {1991}, 148 pp.
- IEC 61400-1 (2005): *Wind Turbines- Part 1: Design requirements*, {2005}, 92 pp.
- Jonkman J., Butterfield S., Musial W., Scott G. (2009): *Definition of a 5-MW Reference Wind Turbine for Offshore System Development*. NREL, Golden, Colorado, USA, 2009, 75 pp.
- ISO 2533 (1978): *Standard Atmosphere*, {1976}, 16 pp.
- Sun, C.T., Quinn, B.J., Tao, J. and Oplinger, D.W. (1996): *Comparative Evaluation of Failure Analysis Methods for Composite Laminates*, NASA, DOT/FAA/AR-95/109, pp. 1-5.
- P. Camanho, P. (2002): *Failure criteria for fibre-reinforced polymer composites.* Department of Applied Mechanics (Mechanical Engineering and Industrial Management), Oporto, Portugal, 2002, pp. 1-3.
- Möllerström E., Ottermo F., Hylander J. and Bernhoff H. (2014): *Eigen frequencies of a vertical axis wind turbine tower made of laminated wood and the effect upon attaching guy wires*. Wind Engineering. Volume 38, No 3, pp 277-289, 2014.
- Carne T.G. (1980): *Guy cable design and damping for vertical axis wind turbines*. Report, Sandia National Laboratories, Albuquerque, NM, USA, 1980.
- Möllerström E. (2015): "Vertical Axis Wind Turbines: Tower dynamics and noise," Master's Thesis, Uppsala University, 2015
- Baral N., Guezenoc H., Davies P. and Balye C. (2008): *High modulus carbon fibre composites: Correlation between transverse tensile and mode I*

interlaminar fracture properties. Material letters, Volume 62, pp 1096-1099, 2008

- Altay O., Butenweg C., Klinkel S., Taddei F. (2014): *Vibration Mitigation of Wind Turbine Towers by Tuned Liquid Column Dampers*. Chair of Structural Analysis and Dynamics, Aachen University, Aachen, Germany, 2014.

- Martynowicz P. (2015): *Vibration control of wind turbine tower-nacelle model with magnetorheological tuned vibration absorber*. AGH University of Science and Technology (Department of Process Control), Krakow, Poland, 2015.

- Armstrong Keith B., Bevan L. Graham, Cole William F. (2005): *Care and Repair of Advanced Composites* (2nd Edition). SAE International. Online version.

- Dr. S. Sttuts, Daniel (2009): *Equivalent viscous damping*. Deparment of Mechanical Engineering, Missouri University of Science and Technology. Available Online at http://web.mst.edu/~stutts/ SupplementalNotes/Eqivalent ViscousDamping.pdf.